Quantum Chaos in Simple Systems

Charles Davis Kocher

Department of Physics

Brown University

A thesis submitted for the degree of

Sc.B. Honors, Mathematical Physics

May 2019

Abstract

We review some aspects of quantum chaos in a variety of systems. We begin with a general discussion of the out-of-time-ordered correlation function, the Maldacena-Shenker-Stanford chaos bound, and the spectral form factor. These ideas are then applied to different Hamiltonians in ordinary quantum mechanics to explore their properties. Additionally, we generalize an existing quantum mechanical calculation of the four-point out-of-time-ordered correlation function for Hamiltonians with discrete spectra to those with continuous spectra. Finally, we study some aspects of quantum chaos in the Sachdev-Ye-Kitaev model. We show that the large q limit of the SYK model yields the Liouville action, and we calculate the four-point function in this limit, showing that the out-of-time-ordered analytic continuation of this correlator saturates the chaos bound. We also calculate the spectral form factor for the SYK model and compare it to the Gaussian Unitary Ensemble random matrix theory analogue.

Contents

List of Figures

Chapter 1

Introduction

In this chapter, we introduce the concept of quantum chaos and the main computational tools used to diagnose a quantum system as choatic. At the end of the chapter, we briefly review the results that will be presented in the remaining chapters.

1.1 Classical Motivation

A major theme of physics since the discovery of quantum mechanics has been studying quantized versions of classical systems. One route from classical physics to quantum mechanics is through the Poisson bracket. In a classical system with generalized position $q(t)$ and corresponding momentum $p(t)$, the Poisson bracket $\{\cdot,\cdot\}_{q(t),p(t)}$ with respect to $q(t)$ and $p(t)$ is

$$\{A,B\}_{q(t),p(t)} = \frac{\partial A}{\partial q(t)}\frac{\partial B}{\partial p(t)} - \frac{\partial A}{\partial p(t)}\frac{\partial B}{\partial q(t)}\,, \tag{1.1}$$

where A and B are any functions of q and p. Stepping to the quantum realm requires relating the commutator $[\cdot,\cdot]$ of operators to the Poisson bracket[1]:

$$[\hat{A},\hat{B}] \equiv \hat{A}\hat{B} - \hat{B}\hat{A} \equiv i\hbar\{A,B\}_{q,p}\,, \tag{1.2}$$

where the Hermitian operators $\hat{A}$ and $\hat{B}$ are the quantum equivalents of the classical quantities A and B [3]. In general, we will be working with time-dependent Heisenberg operators $\hat{A}(t)$, which are related to the time-independent Schrödinger operators[2] $\hat{A} \equiv \hat{A}(0)$ by

[1] To ensure that the multiplicative constant is correct, it is easy to see that Equation (1.2) implies $[\hat{q},\hat{p}] = i\hbar$, as expected.

[2] Note that throughout this work $\hat{A}(0)$ and $\hat{A}$ will be used interchangeably because of their equivalence.

$$\hat{A}(t) = e^{i\hat{H}t}\hat{A}e^{-i\hat{H}t} \ , \tag{1.3}$$

when the Hamiltonian $\hat{H}$ is time-independent.

The goal now is to understand quantum chaos. One way we can approach the problem is to relate classical chaos to a Poisson bracket and then use Equation (1.2) to gain insight into the quantum analogue. Classically, a chaotic system is one that is incredibly sensitive to initial conditions. To set up a precise definition, consider two one-dimensional classical particles, with positions $q_1(t)$ and $q_2(t)$, under the influence of some potential. Let the initial conditions be such that

$$\delta q(0) \equiv q_1(0) - q_2(0) \ll 1 \ . \tag{1.4}$$

This system is chaotic if the initial behavior is described by

$$\delta q(t) = \delta q(0) e^{\lambda_L t} \ ; \tag{1.5}$$

that is, the difference between the positions of the particles grows exponentially. The constant λ_L is known as the Lyapunov exponent of the system.

Equation (1.5) leads to a diagnostic for quantum chaos. First, rewrite it by dividing by $\delta q(0)$: $\delta q(t)/\delta q(0) = e^{\lambda_L t}$. The left side of this equation can be interpreted as the derivative $\frac{\partial q(t)}{\partial q(0)}$, which can be conveniently expressed as a Poisson bracket:

$$\{q(t), p(0)\}_{q(0),p(0)} = \frac{\partial q(t)}{\partial q(0)}\frac{\partial p(0)}{\partial p(0)} - \frac{\partial q(t)}{\partial p(0)}\frac{\partial p(0)}{\partial q(0)} = \frac{\partial q(t)}{\partial q(0)} \ , \tag{1.6}$$

since the second term in the middle expression is zero. Using Equation (1.2) directly now would result in an operator. The expectation value of this operator would give an exponentially growing function of time, but it turns out that the thermal expectation value at inverse temperature $\beta = 1/T$, defined as

$$\langle \hat{A} \rangle \equiv \frac{1}{Z(\beta)} \mathrm{Tr}\left[e^{-\beta\hat{H}}\hat{A}\right] \ , \tag{1.7}$$

where $Z(\beta) \equiv \mathrm{Tr}\left[e^{-\beta\hat{H}}\right]$, is zero because of the cancellation of phases [4, 5]. This problem can be easily remedied by simply taking the expectation value of the square of the commutator. Applying Equation (1.2), we find

$$\left\langle [\hat{q}(t), \hat{p}(0)]^2 \right\rangle \sim \hbar^2 e^{2\lambda_L t} \ . \tag{1.8}$$

We now examine the terms on the left side of Equation (1.8). A typical term is of the form $\langle \hat{q}(t)\hat{p}(0)\hat{q}(t)\hat{p}(0)\rangle$. The form of this expectation value can be generalized

to two time-dependent operators $\hat{A}(t)$ and $\hat{B}(t)$, such that a condition for quantum chaos is

$$\langle \hat{A}(t)\hat{B}(0)\hat{A}(t)\hat{B}(0)\rangle \sim e^{2\lambda_L t} \, . \tag{1.9}$$

The objects $\langle \hat{A}(t)\hat{B}(0)\hat{A}(t)\hat{B}(0)\rangle$ and $\langle [\hat{q}(t), \hat{p}(0)]^2\rangle$ are both referred to as four-point out-of-time-ordered correlation functions (OTOC). Both are used to detect quantum chaos; they will be one of the main objects of study.

1.2 The Chaos Bound

Maldacena, Shenker, and Stanford established a bound of $\frac{2\pi}{\beta}$ on the Lyapunov exponent[3] for any system exhibiting quantum chaos [6]. The inspiration for conjecturing the bound was that, in a large N CFT holographically described by Einstein gravity, the Lyapunov exponent was found to be precisely $\frac{2\pi}{\beta}$ [7]. Proving the quantum chaos result relies on a preliminary exercise in complex analysis. Suppose we have a real-valued function $f(t)$, where $f(z)$ is analytic in the half-strip region $\mathrm{Re}(z) < 0$, $-\beta/4 \leq \mathrm{Im}(z) \leq \beta/4$ and the magnitude $|f(z)| \leq 1$ for any such $z = t + i\tau$ in this region. Then this function satisfies

$$\frac{1}{1-f}\left|\frac{df}{dt}\right| \leq \frac{2\pi}{\beta} + O\left(e^{-4\pi t/\beta}\right) \, . \tag{1.10}$$

Why is this result important? Consider $f(z) = 1 - \epsilon e^{\lambda_L z}$. The absolute value of the derivative is λ_L times $1-f$, such that the inequality above reduces to $\lambda_L \leq \frac{2\pi}{\beta}$. Thus, if we can prove Equation (1.10) and that the four-point OTOC has the form $1-\epsilon e^{\lambda_L z}$, then we have proved the chaos bound.

First, the proof of the inequality. Let $z = t + i\tau$ and consider the change of coordinates

$$w = \frac{1 - \sinh\left(\frac{2\pi}{\beta}(t+i\tau)\right)}{1 + \sinh\left(\frac{2\pi}{\beta}(t+i\tau)\right)} \, , \tag{1.11}$$

which maps the half-strip to the unit disk. As a composition of analytic functions, w is analytic. Define $F(w(t+i\tau)) \equiv f(t+i\tau)$. This function[4] is analytic because f

[3] If you look at the definitions of the previous section and compare them to the calculation of this section, you will see a factor of 2 difference in the definition of the Lyapunov exponent. The convention in this section is the standard for discussions of quantum chaos.

[4] We are simply using the half-strip as a parameterization of the unit disk in order to define f there.

and w are, and it maps the unit disk to the unit disk since the absolute value of f is bounded by 1. The Schwarz-Pick theorem (see Appendix A) states that any analytic function from the unit disk to the unit disk either preserves or decreases distances in the hyperbolic metric, which is given by

$$ds^2 = \frac{4|dz|^2}{(1-|z|^2)^2} \, . \tag{1.12}$$

Applying this fact to F and w and taking a square root gives

$$\frac{|dF|}{1-|F(w)|^2} \leq \frac{|dw|}{1-|w|^2} \, . \tag{1.13}$$

We now restrict our attention to the $\tau = 0$ axis. Dividing both sides by dt and identifying $F(w)$ with $f(t)$ (since τ is now zero), we find

$$\frac{1}{1-|f(t)|^2} \left| \frac{df}{dt} \right| \leq \frac{1}{1-|w|^2} \left| \frac{dw}{dt} \right| \, . \tag{1.14}$$

Since f is real on the real axis, we can factor the denominator on the left-hand side. The right-hand can be calculated, such that

$$\frac{1}{1-f} \left| \frac{df}{dt} \right| \leq \frac{2\pi}{\beta} \coth \frac{2\pi t}{\beta} \frac{(1+f)}{2} \leq \frac{2\pi}{\beta} + O(e^{-4\pi t/\beta}) \, , \tag{1.15}$$

which is what we set out to prove.

Returning to physics, we now state the chaos bound. Let $y^4 = \frac{1}{Z} e^{-\beta H}$. Then, we can define the four-point OTOC between two operators W and V as

$$F(t) = \mathrm{Tr}[yVyW(t)yVyW(t)] \, , \tag{1.16}$$

and we can define the factorized version as

$$F_d = \mathrm{Tr}\left[y^2 V y^2 V\right] \mathrm{Tr}\left[y^2 W(t) y^2 W(t)\right] \, . \tag{1.17}$$

The chaos bound is the statement that

$$\frac{d}{dt}(F_d(t) - F(t)) \leq \frac{2\pi}{\beta}(F_d(t) - F(t)) \tag{1.18}$$

We will heuristically explain why this should be true. At intermediate times, $F(t)$ should be close to $F_d(t)$; at these times, correlators such as $\langle VVW(t)W(t)\rangle$ approach their factorized values as well. However, the OTOC is special, in that $F(t)$ cannot remain constant because quantum chaotic systems scramble information. Thus, $F(t)$

develops a commutator term and decreases. A general expectation for chaotic systems (as we saw above) is that growth is exponential, so the difference should roughly obey

$$F_d(t) - F(t) = \epsilon e^{\lambda_L t} \ . \tag{1.19}$$

Applying the mathematical result above to this functional form gives the chaos bound.

1.3 Spectral Form Factors

In studies of black holes and other chaotic systems, random matrix theory provides one route for a tractable analysis, while the OTOC of the previous sections provides another. The relationship between quantum chaos and random matrix theory is more general: the quantum chaos conjecture states that all quantum chaotic systems should be describable by a random matrix theory model consistent with the system's symmetries [8]. The spectral form factor, explored in detail in [1], illuminates the random matrix theory properties of a quantum chaotic system. The OTOC, as we would expect from the classical analogue, only describes the behavior of the system at early times and is a quantum mechanical construct [9]. In contrast, the spectral form factor also captures the late-time behavior of a system and its statistical properties [10]. The late-time behavior of the spectral form factor will turn out to be related to the discreteness of the spectrum of the Hamiltonian.

First, we define an important analytic continuation of the partition function $Z(\beta) = \mathrm{Tr}\left[e^{-\beta H}\right]$ for a system at time t and inverse temperature β as

$$Z(\beta, t) \equiv \mathrm{Tr}\left[e^{-\beta H - iHt}\right] \ , \tag{1.20}$$

where we have continued β to $\beta + it$. The time average of $Z(\beta, t)$ vanishes, so it is an oscillating function around zero. The size of fluctuations can be determined from normalizing by the partition function:

$$g(\beta, t) \equiv \left| \frac{Z(\beta, t)}{Z(\beta)} \right|^2 \ . \tag{1.21}$$

The function $g(\beta, t)$ is the spectral form factor[5]. For our preliminary analysis, we will begin by expanding the two traces in the numerator of the definition of the spectral form factor in terms of the (assumed to be discrete) energy eigenbasis:

[5] Although, as we will see, most studies use the *annealed*, disorder-averaged (see Equation (3.50)) version of this quantity as the spectral form factor. The normalization is also optional.

$$\left|\frac{Z(\beta,t)}{Z(\beta)}\right|^2 = \frac{1}{|Z(\beta)|^2}\sum_{m,n} e^{-\beta(E_m+E_n)}e^{it(E_m-E_n)} \ . \tag{1.22}$$

The sum here is over all eigenvalues, including multiplicities. The final factor gives a way to proceed, because if t was large then it would collapse to a Kronecker delta. Indeed, taking the long time average gives

$$\lim_{T\to\infty}\frac{1}{T}\int_0^T dt g(\beta,t) = \frac{1}{|Z(\beta)|^2}\sum_E N_E^2 e^{-2\beta E} \ , \tag{1.23}$$

where the sum here goes over all energy levels, and the multiplicity is accounted for in the factor N_E. If $N_E = 1$ for all E, then this final sum is just the definition of $Z(2\beta)$. The long-time average, then, is non-zero for a system with a discrete spectrum. What happens for a continuous spectrum? It turns out that the long time average is zero, such that the spectral form factor decays to zero.

1.3.1 Examples

We now consider two simple examples to illustrate the above points. First, the harmonic oscillator. Instead of treating the two traces in the numerator of the spectral form factor together as in Equation (1.22), we now consider them separately. Since $E_n = n + 1/2$ for the harmonic oscillator, we can calculate, for constant α,

$$\mathrm{Tr}\left[e^{\alpha H}\right] = \sum_{n=0}^{\infty} e^{\alpha(n+1/2)} = e^{\alpha/2}\sum_{n=0}^{\infty}(e^{\alpha})^n = \frac{e^{\alpha/2}}{1-e^{\alpha}} \ . \tag{1.24}$$

We can now use this general result to find

$$g(\beta,t) = \frac{\left(\frac{e^{-(\beta+it)/2}}{1-e^{-(\beta+it)}}\right)\left(\frac{e^{-(\beta-it)/2}}{1-e^{-(\beta-it)}}\right)}{\left(\frac{e^{-\beta/2}}{1-e^{-\beta}}\right)^2} = \frac{1+e^{-2\beta}-2e^{-\beta}}{1+e^{-2\beta}-2e^{-\beta}\cos(t)} \ . \tag{1.25}$$

This spectral form factor is plotted for $\beta = 5$ in Figure 1.1. The notable feature is the late-time oscillations about a positive number, as claimed in the derivation of the general behavior of the long time average.

Now we take a toy[6] system with continuous eigenvalues distributed in such a way that the trace in the energy eigenbasis is

$$\mathrm{Tr}\left[e^{\alpha H}\right] = \int_0^{\infty}\langle E|E\rangle\, dE e^{-\alpha E} = \frac{1}{\alpha}\langle E|E\rangle \ , \tag{1.26}$$

[6]Non-physical. Here we are only concerned with the mathematical result.

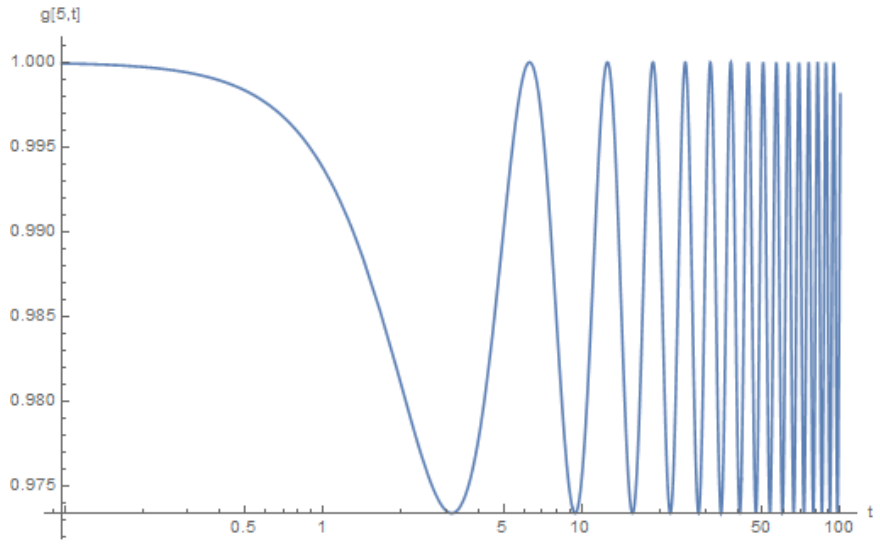

Figure 1.1: A plot of the spectral form factor for the harmonic oscillator with $\beta = 5$. The long time average is non-zero, as is generally the case for systems with a discrete eigenvalue spectrum.

where we have assumed that $\mathrm{Re}(\alpha) > 0$ and all of the energy eigenstates are normalized in the same way. This (seemingly infinite) normalization cancels by the division in the definition of the spectral form factor, so we will ignore it. Thus, for this system, the spectral form factor is

$$g(\beta, t) = \frac{\beta^2}{\beta^2 + t^2} \ . \tag{1.27}$$

This spectral form factor with $\beta = 5$ is plotted in Figure 1.2. As claimed, the long time average is zero, and the spectral form factor decays to zero as $t \to \infty$. Furthermore, even if the system we are considering has a discrete number of energy eigenstates, if the eigenvalues are distributed closely enough that we can treat sums over the eigenvalues as "coarse-grained" integrals[7], we expect the early-time behavior of the spectral form factor to be as shown here.

1.4 Summary of Results

Now that we have presented the tools we will use to study quantum chaos, we will list our main results. In the next chapter, we will study OTOC in the familiar setting of quantum mechanics and do explicit calculations for some quantum systems, following [9]. We will also generalize the method of [9] to Hamiltonians with continuous energy

[7] This criterion applies for the GUE and SYK models considered later.

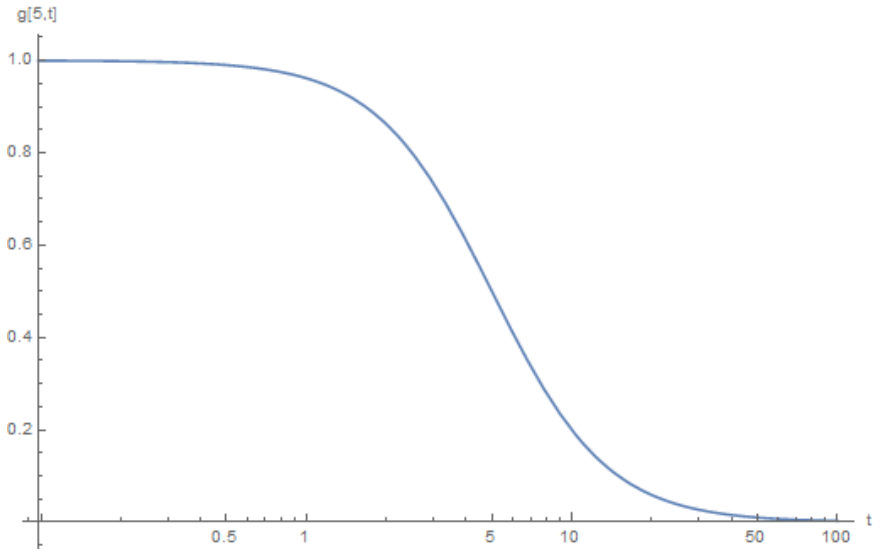

Figure 1.2: A plot of the spectral form factor for a system with a continuous spectrum with $\beta = 5$. The long time average is zero in this case, as expected.

spectra. In the third chapter, we focus on the SYK model, following [2, 11, 12, 13]. We describe the model and its connection to the Liouville action in the large q limit, then compute the four-point function in this limit. We show that the four-point OTOC saturates the chaos bound when $v \to 1$. We then describe the relationship between the SYK model and the GUE random matrix model. The numerically-calculated spectral form factors of each are compared, then the GUE spectral form factor is analytically computed. We finish with some concluding remarks about other quantum chaotic systems and recent developments in the field. The appendices include a proof of the Schwarz-Pick Theorem used in the mathematical result that led to the chaos bound and a full listing of all the code used to generate the figures in this paper.

Chapter 2

Quantum Chaos in Quantum Mechanics

In this chapter, we build the formalism for calculating OTOC in the setting of quantum mechanics. Doing easy quantum mechanical calculations will give some basic intuition and preliminary insight into how to approach OTOC and how to interpret their actual values.

2.1 Calculating OTOC in Quantum Mechanics

In [9], a method for calculating the four-point OTOC at temperature T,

$$C_T(t) \equiv -\langle [\hat{q}(t), \hat{p}(0)]^2 \rangle \ , \tag{2.1}$$

is presented for quantum mechanical systems described by a Hamiltonian with a discrete spectrum. This is an ideal starting place for an exploration of the various behaviors of OTOC, because quantum mechanical calculations are generally much simpler than quantum field theory calculations and discrete spectra are easier to work with than continuous spectra.

To proceed, first use the eigenstates $|n\rangle$ of the Hamiltonian to express the trace in the definition of $C_T(t)$:

$$C_T(t) = -\frac{1}{Z(\beta)} \sum_n \langle n| \, e^{-\beta \hat{H}} [\hat{q}(t), \hat{p}(0)]^2 \, |n\rangle \ . \tag{2.2}$$

Defining the energy eigenvalues as $\hat{H} \, |n\rangle \equiv E_n \, |n\rangle$, Equation (2.2) can be rewritten as

$$C_T(t) = \frac{1}{Z(\beta)} \sum_n e^{-\beta E_n} c_n(t) \ , \tag{2.3}$$

where the microcanonical OTOC $c_n(t)$, defined as

$$c_n(t) \equiv -\langle n| \left[\hat{q}(t), \hat{p}(0)\right]^2 |n\rangle \ , \tag{2.4}$$

has been introduced. Note that $C_T(t)$ is just the thermal average of all of the microcanonical OTOC.

The next step toward finding a useful form for the OTOC is to insert a complete set of energy eigenstates, $\hat{I} = \sum_m |m\rangle \langle m|$, between the two commutators in Equation (2.4), yielding

$$c_n(t) = \sum_m b_{nm}(t) b^*_{nm}(t) \ , \tag{2.5}$$

$$b_{nm}(t) = -i \langle n| \left[\hat{q}(t), \hat{p}(0)\right] |m\rangle \ . \tag{2.6}$$

The matrix $\mathbf{b(t)}$ with matrix elements $b_{nm}(t)$ is a Hermitian matrix, since $b^*_{nm}(t) = i \langle m| \left[\hat{p}(0), \hat{x}(t)\right] |n\rangle = -i \langle m| \left[\hat{x}(t), \hat{p}(0)\right] |n\rangle = b_{mn}(t)$ implies $\mathbf{b(t)}^\dagger = \mathbf{b(t)}$.

The quantity $b_{nm}(t)$ has two terms; consider the first one. By inserting another complete set of energy eigenstates after $\hat{q}(t)$, the first term becomes

$$\langle n| e^{i\hat{H}t} \hat{q}(0) e^{-i\hat{H}t} \hat{p}(0) |m\rangle = \sum_k e^{i(E_n - E_k)t} q_{nk} p_{km} \ , \tag{2.7}$$

where $q_{nk} \equiv \langle n| \hat{q}(0) |k\rangle$ and $p_{km} \equiv \langle k| \hat{p}(0) |m\rangle$ are the matrix elements of the position and momentum operators in the energy representation. Combining Equations (2.6) and (2.7) yields

$$b_{nm}(t) = -i \sum_k \left(e^{i(E_n - E_k)t} q_{nk} p_{km} - e^{i(E_k - E_m)t} p_{nk} q_{km} \right) \ . \tag{2.8}$$

The matrix elements of $\hat{q}$ are much easier to work with numerically, so it would be preferable to write Equation (2.8) with only them. If the Hamiltonian is of the form

$$\hat{H} = \frac{1}{2}\hat{p}^2 + V(\hat{q}) \ , \tag{2.9}$$

then $[\hat{H}, \hat{q}] = \frac{1}{2}[\hat{p}^2, \hat{q}] = -i\hat{p}$ implies, upon taking matrix elements,

$$p_{nm} = i(E_n - E_m) q_{nm} \ . \tag{2.10}$$

Plugging this form for p_{nm} back into Equation (2.8) yields the final form for $b_{nm}(t)$:

$$b_{nm}(t) = \sum_k q_{nk} q_{km} \left[(E_k - E_m) e^{i(E_n - E_k)t} - (E_n - E_k) e^{i(E_k - E_m)t} \right] \ . \tag{2.11}$$

Plugging Equation (2.11) back into Equation (2.5), and subsequently back into Equation (2.3) yields the important final form of the four-point OTOC:

$$\begin{aligned} C_T(t) = \frac{1}{Z(\beta)} \sum_{n,m,k,j} e^{-\beta E_n} \left[q_{nk} q_{km} \left(E_{km} e^{iE_{nk}t} - E_{nk} e^{iE_{km}t} \right) \right] \\ \times \left[q_{mj} q_{jn} \left(E_{jn} e^{iE_{mj}t} - E_{mj} e^{iE_{jn}t} \right) \right] \ , \end{aligned} \tag{2.12}$$

where the four sums are over all energy eigenstates $|n\rangle$ with corresponding energy E_n of the Hamiltonian $\hat{H} = \frac{1}{2}\hat{p}^2 + V(\hat{q})$, and $q_{nk} \equiv \langle n| \hat{q} |k\rangle$, $E_{nm} \equiv E_n - E_m$.

2.1.1 The Harmonic Oscillator

As is the case with most concepts in quantum mechanics, the best explicit calculation to carry out first involves the harmonic oscillator. Recall that for the harmonic oscillator with $m = 1$,

$$\hat{H} = \frac{1}{2}\hat{p}^2 + \frac{1}{2}\omega^2 \hat{q}^2 = \omega \left(\hat{a}^\dagger \hat{a} + \frac{1}{2} \right) \ , \tag{2.13}$$

$$\hat{a}^\dagger |n\rangle = \sqrt{n+1}\, |n+1\rangle \ , \ \ \hat{a} |n\rangle = \sqrt{n}\, |n-1\rangle \ , \tag{2.14}$$

$$\hat{q} = \frac{1}{\sqrt{2\omega}} \left(\hat{a}^\dagger + \hat{a} \right) \ , \tag{2.15}$$

where $\hat{H}$ is the Hamiltonian[1], $\hat{a}$ and $\hat{a}^\dagger$ are the annihilation and creation operators, and the energy eigenstates are $|n\rangle$ for $n = 0, 1, 2, \ldots$, with energies $E_n = \omega \left(n + \frac{1}{2} \right)$.

Using Equation (2.15), we can calculate q_{nm}:

$$q_{nm} = \frac{1}{\sqrt{2\omega}} \langle n| \left(\hat{a}^\dagger + \hat{a} \right) |m\rangle = \frac{1}{\sqrt{2\omega}} \left(\sqrt{m}\delta_{n,m-1} + \sqrt{m+1}\delta_{n,m+1} \right) \ . \tag{2.16}$$

It is easiest to plug this result into Equation (2.11) and find $b_{mn}(t)$ first because of its particularly simple form. Multiplying two of the three resulting binomials yields

[1] We have set $\hbar = 1$ for convenience.

$$
\begin{aligned}
b_{nm}(t) = \frac{1}{2\omega}\sum_{k=0}^{\infty}(&\sqrt{k}\sqrt{m}\delta_{n,k-1}\delta_{k,m-1} + \sqrt{k+1}\sqrt{m}\delta_{n,k+1}\delta_{k,m-1} \\
&+ \sqrt{k}\sqrt{m+1}\delta_{n,k-1}\delta_{k,m+1} + \sqrt{k+1}\sqrt{m+1}\delta_{n,k+1}\delta_{k,m+1}) \\
&\times \left(E_{km}e^{iE_{nk}t} - E_{nk}e^{iE_{km}t}\right) \ .
\end{aligned} \tag{2.17}
$$

Upon multiplying the final binomial through, using the Kronecker deltas to rewrite each quantity in terms of only the m index, and evaluating the sum over k, we find that the first and fourth terms are individually zero and that the second and third terms give

$$
\begin{aligned}
2\omega b_{nm}(t) = m\delta_{n,m}&(E_{(m-1)m}e^{iE_{m(m-1)}t} - E_{m(m-1)}e^{iE_{(m-1)m}t}) \\
&+ (m+1)\delta_{n,m}(E_{(m+1)m}e^{iE_{m(m+1)}t} - E_{m(m+1)}e^{iE_{(m+1)m}t}) \ .
\end{aligned} \tag{2.18}
$$

Noting that $E_{(m-1)m} = -\omega$ and $E_{m(m-1)} = \omega$, the two terms proportional to m cancel, leaving only

$$
b_{nm}(t) = \delta_{n,m}\cos(\omega t) \ . \tag{2.19}
$$

Since $b_{nm}(t)$ is real, $\mathbf{b}$ is a symmetric matrix, meaning $c_n(t) = \cos^2(\omega t)$: the microcanonical OTOC is constant as a function of energy. Its thermal average is then just itself, giving the final result

$$
C_T(t) = \cos^2(\omega t) \ , \tag{2.20}
$$

for the harmonic oscillator.

Some comments are in order. First, the four-point OTOC for the harmonic oscillator does not grow exponentially; as expected, the harmonic oscillator is not an example of a quantum chaotic system. Indeed, it would be strange if the simplest quantum system was chaotic, for then quantum chaos would not be a special property. Moreover, the classical harmonic oscillator is not chaotic. It would be unexpected for the harmonic oscillator to become chaotic upon quantization. Second, the OTOC can be calculated in other ways, all of which give the same result.

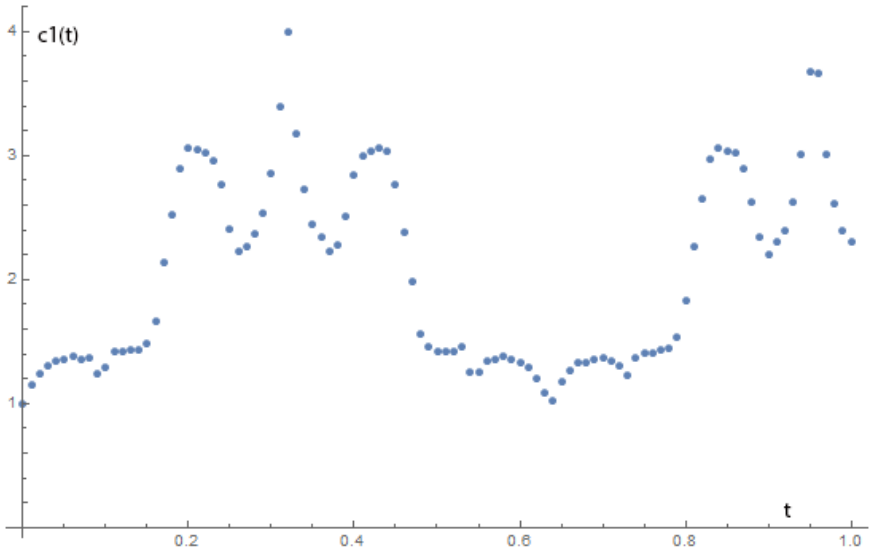

Figure 2.1: A plot of the numerically calculated microcanonical OTOC for the $n = 1$ energy level of the particle in a box Hamiltonian.

2.1.2 Particle in a Box

The second typical example of any quantum mechanical behavior is the particle in a box. Here, the Hamiltonian is defined as $\hat{H} = \hat{p}^2/2$ on an interval of length L centered at x_c and infinite elsewhere. The energy eigenfunctions are

$$\psi_n(x) = \sqrt{\frac{2}{L}} \sin\left(\frac{n\pi(x - x_c + \frac{L}{2})}{L}\right) , \tag{2.21}$$

with energies $E_n = \frac{n^2\pi^2}{2L}$, where $n = 1, 2, \ldots$ denote the energy levels. The matrix elements q_{kt} can be calculated using Mathematica to be

$$q_{kt} = \frac{4(-1 + (-1)^{k+t})kt}{\pi^2(k-t)^2(k+t)^2} , \tag{2.22}$$

when $k \neq t$ and $q_{kk} = 1/2$. Using this result, we can numerically calculate the microcanonical OTOC; the function $c_1(t)$ is shown in Figure 2.1. From here, we could continue to calculate the full OTOC, but for this we refer[2] to [9]. The result, of course, is that the particle in a box does not exhibit quantum chaos.

2.1.3 The Free Particle

Now we want to move beyond systems with a discrete spectrum. The simplest such Hamiltonian with a continuous spectrum is the free particle with $\hat{H} = \frac{1}{2}\hat{p}^2$. We could

[2]Many more interesting examples are given in [9] as well, which we omit here.

extend the previous analysis to the continuous case and proceed that way, but there is a shorter route to the answer. We will take up the more general analysis in the next section.

The trick for this Hamiltonian[3] is to notice that the commutator $[e^{\pm i\hat{H}t}, \hat{p}]$ is zero. Then, we can pull the exponentials that arise from the definition of $\hat{x}(t)$ out of the commutator with $\hat{p}$, leaving

$$[\hat{x}(t), \hat{p}] = e^{i\hat{H}t}[\hat{x}, \hat{p}]e^{-i\hat{H}t} = i\hbar \ . \tag{2.23}$$

The thermal average of a constant is just a constant, so the four-point OTOC for the free particle is

$$C_T(t) = \hbar^2 \ . \tag{2.24}$$

2.2 Continuous Spectra

Our calculation of the four-point OTOC for the free particle made no mention of the spectrum of the Hamiltonian; it instead focused on the operator algebra. This process led to an unambiguous result. We now try to generalize the analysis of the first section of this chapter to systems with a continuous spectrum.

The first obvious difficulty that arises when dealing with a continuous spectrum of eigenstates $|E\rangle$ of the Hamiltonian H is the normalization. We now assume that the states are delta function normalized:

$$\langle E|E'\rangle = \delta(E - E') \ . \tag{2.25}$$

From our work with the spectral form factor of a system with a continuous spectrum in the Introduction, we expect this normalization to cancel out at the end of our calculation because every trace we take is proportional to $\delta(0)$. To show this more explicitly, if we take the expression $q_{nk}q_{km}q_{mj}q_{jn}$, which arises as the general form of a term in the sum of Equation (2.12), we would get four delta functions and four integrals; roughly, $q_{nk}q_{km}q_{mj}q_{jn} \sim \delta(E_n - E_k)\delta(E_k - E_m)\delta(E_m - E_j)\delta(E_j - E_n)$. Doing the four integrals would set the different energy variables equal to each other one-by-one, until the final integral, where the remaining delta function would be $\delta(E_n - E_n) = \delta(0)$. This is the normalization factor that cancels with the immediate $\delta(0)$ that comes from the simpler trace in the denominator.

[3]This trick will work for any Hamiltonian that is purely a function of $\hat{p}$

The second question we may have when we use a continuous spectrum of eigenvalues is how the identity operator (which we used repeatedly in the previous section) might change. If we use the above normalization for the eigenstates, the identity operator is just[4] $\hat{I} = \int dE \, |E\rangle \langle E|$. Let's see an example of this. For the free particle, the eigenstates are $|E, \mathrm{sgn(p)}\rangle = N(E) \, |p\rangle$, where $N(E)$ is a normalization constant, with eigenvalues $E = \frac{p^2}{2}$. To find the correct normalization, we compute

$$\langle E, a|E', b\rangle = \int \frac{dx}{2\pi} N(E)N(E')e^{ix(p'-p)} = N(E)N(E')\delta(p-p') \; , \tag{2.26}$$

where a and b represent which copy of E (right- or left-moving) we are referencing[5]. Now, we use the fact that $p = \pm\sqrt{2E}$ and the identity $\delta(g(x)) = \frac{1}{|g(x_0)|}\delta(x - x_0)$, where $g(x_0) = 0$, to see that

$$N(E)N(E')\delta(p-p') = N(E)N(E')\delta(\sqrt{2E} - \sqrt{2E'}) = N(E)^2\sqrt{2E}\delta(E-E') \; . \tag{2.27}$$

Since we want $\langle E|E'\rangle = \delta(E - E')$, we choose $N(E) = \frac{1}{(2E)^{1/4}}$. We can check this answer does not change the identity operator by using the known result for momentum completeness and the change of variables $p = \pm\sqrt{2E}$:

$$\begin{aligned} \langle x|x'\rangle &= \int_{-\infty}^{\infty} \frac{dp}{2\pi} e^{ip(x-x')} = 2\int_0^{\infty} \frac{dE}{2\pi} \frac{1}{\sqrt{2E}} e^{i\sqrt{2E}(x-x')} \\ &= \int_0^{\infty} dE \, \langle x|E,+\rangle \langle E,+|x'\rangle + \int_0^{\infty} dE \, \langle x|E,-\rangle \langle E,-|x'\rangle \\ &= \langle x| \, \hat{I} \, |x'\rangle = \delta(x-x') \end{aligned} \tag{2.28}$$

Because of the above discussion, we can write down the analogue of $C_T(t)$ by merely interpreting the discrete energy variables as continuous ones:

$$\begin{aligned} C_T(t) = \frac{1}{Z(\beta)} \int dE_n dE_m dE_k dE_j \; e^{-\beta E_n} \left[q_{nk} q_{km} \left(E_{km} e^{iE_{nk}t} - E_{nk} e^{iE_{km}t} \right) \right] \\ \times \left[q_{mj} q_{jn} \left(E_{jn} e^{iE_{mj}t} - E_{mj} e^{iE_{jn}t} \right) \right] \; , \end{aligned} \tag{2.29}$$

where all variables are defined as before. While we are not going to do a calculation with this formula, we will now describe a few of the features of one with the free

[4]Notice that this statement holds for both $\hat{q}$ and $\hat{p}$, the prototypical operators with continuous spectra.

[5]Notice that there could be a $\delta_{a,b}$ in the result as well, but it is also taken care of by the delta function.

particle. First, the q_{nk} are going to be differential operators: this is because the matrix elements of the $\hat{q}$ operator are derivatives with respect to p in the momentum basis, and our energy eigenbasis is just the momentum basis. We would also have a delta function in this matrix element, confirming our above discussion of the normalization.

Chapter 3

The SYK Model

We will now discuss one of the most studied systems that exhibits quantum chaos: the Sachdev-Ye-Kitaev (SYK) model, consisting of N Majorana fermions interacting with a q-at-a-time random coupling, where, in the limit of strong coupling, the system has a near conformal symmetry. We will see that the four-point function of the SYK model saturates the MSS chaos bound. In particular, we will focus on the $O(1/N)$ part of the $q = \infty$ four-point function and the spectral form factor, following [1], [2], and [11].

3.1 The Model

The SYK model describes a system of N Majorana fermions with interactions involving q fermions at a time with Gaussian-random coupling constants, where we will take q to be even[1]. Explicitly, the Hamiltonian is

$$H = (i)^{\frac{q}{2}} \sum_{1 \leq i_1 < i_2 < \cdots < i_q \leq N} j_{i_1 i_2 \ldots i_q} \psi_{i_1} \psi_{i_2} \cdots \psi_{i_q} \ , \tag{3.1}$$

where ψ_k are Majorana fermions, with $k = 1, \ldots, N$, and the coupling constants $j_{i_1 i_2 \ldots i_q}$ are drawn from a Gaussian distribution with mean zero and variance given in terms of the dimensionful parameter J:

$$\langle j^2_{i_1 i_2 \ldots i_q} \rangle = \frac{J^2 (q-1)!}{N^{(q-1)}} \ . \tag{3.2}$$

We are interested in the four-point function of this theory; to get it, we will first discuss some results concerning the Euclidean time two-point function, which is given by

[1] This section follows [11].

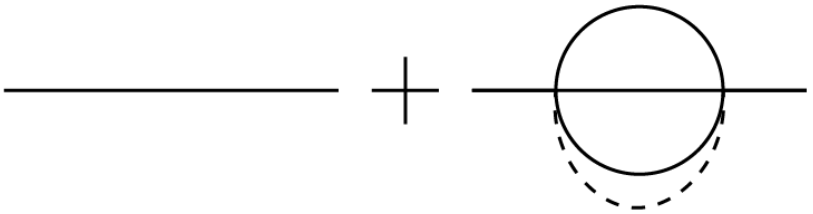

Figure 3.1: The propagator and first correction for the $q = 4$ SYK model. The dashed line in the watermelon diagram represents the disorder average. The vertices in the melon diagram do not add any powers of N to the propagator, so the leading order contribution is simply the sum of all iterated wateremelon diagrams.

$$G(\tau) = \langle T[\psi_i(\tau)\psi_i(0)]\rangle \equiv \langle \psi_i(\tau)\psi_i(0)\rangle\theta(\tau) - \langle \psi_i(0)\psi_i(\tau)\rangle\theta(-\tau) \ , \tag{3.3}$$

where T is the time-ordering symbol, defined with the conventional minus sign for fermions. In the free case, the propagator is[2]

$$G_f(\tau) = \frac{1}{2}\text{sgn}(\tau) \ . \tag{3.4}$$

In the interacting theory, we would like to compute corrections to this propagator. To simplify matters, we only want to consider the leading order in N and will disorder average over pairs of vertices[3]. So the first correction to the two-point function we will consider is the "watermelon" diagram shown for the case $q = 4$ in Figure 3.1. The incoming and outgoing fermions must have the same index i (otherwise we would be considering an interaction and not a correction to the free propagator, which must have the incoming and outgoing fermions the same), so there are in general $q - 1$ propagators between the vertices. Each vertex, then, contributes a factor of $j_{i_1\ldots i_{(q-1)}i}$ (up to a re-ordering of these indices depending on where i falls in relation to the others). These two factors are multiplied and then averaged over the $q - 1$ undetermined fermions, giving a vertex contribution of

$$\sum_{i_1,i_2,\ldots,i_{(q-1)}} \langle j^2_{i_1\ldots i_{(q-1)}i}\rangle \sim N^{(q-1)}\frac{J^2(q-1)!}{N^{(q-1)}} \ , \tag{3.5}$$

where the factors of N in the numerator come from the sum and the factors of N in the denominator come from the variance of the couplings. Accordingly, the watermelon

[2]The sign function is defined by $\text{sgn}(\tau) = \tau/|\tau|$ when τ is non-zero and $\text{sgn}(0) = 0$.

[3]A disorder average over a single vertex would be the mean of $j_{i_1 i_2\ldots i_q}$, which is zero, so we need only consider even numbers of vertices.

diagram contributes to the interacting propagator at the same order in N as the free propagator.

The general case is not too different, where we just consider one-particle-irreducible diagrams made from these watermelons, the "iterated watermelon" diagrams. In the strong-coupling (conformal) limit, the full propagator at finite inverse temperature β is given by

$$G_c(\tau) = b\left[\frac{\pi}{\beta \sin\frac{\pi\tau}{\beta}}\right]^{2\Delta} \mathrm{sgn}(\tau)\ , \tag{3.6}$$

where $\Delta = 1/q$ and $J^2 b^q \pi = \left(\frac{1}{2} - \Delta\right)\tan(\pi\Delta)$. Since the conformal symmetry is not exact, there will be a correction to this two-point function. If we define $\mathcal{J}^2 \equiv \frac{q}{2^{(q-1)}} J^2$, we can compute the perturbation expansion (in powers of $\frac{1}{\beta\mathcal{J}}$) of the large q two point function. The resulting functional form is

$$G(\tau) = G_c(\tau)\left[1 + \frac{g(\tau)}{q} + \dots\right]\ . \tag{3.7}$$

3.1.1 The Four-Point Function

We will now consider the $O(1/N)$ piece of the four-point function for the SYK model at strong coupling. The indices of the external fermions must be pairwise equal because of the disorder sum. For simplification reasons, we will work with the averaged correlator, which is defined to be

$$G^{(4)}(\tau_1,\tau_2,\tau_3,\tau_4) = \frac{1}{N^2}\sum_{i,j=1}^{N}\langle T[\psi_i(\tau_1)\psi_i(\tau_2)\psi_j(\tau_3)\psi_j(\tau_4)]\rangle\ . \tag{3.8}$$

We can expand $G^{(4)}$ in powers of $1/N$. The leading diagram, which is shown in Figure 3.2, simply propagating from τ_1 to τ_2 and from τ_3 to τ_4, is of order 1, since for all pairs (i,j), the diagram just evaluates to[4] $G(\tau_{12})G(\tau_{34})$. The sum over N^2 different combinations cancels the $1/N^2$ from the average. This is the only piece of $O(1)$, so we can write

$$G^{(4)}(\tau_1,\tau_2,\tau_3,\tau_4) = G(\tau_{12})G(\tau_{34}) + \frac{1}{N}\mathcal{F}(\tau_1,\tau_2,\tau_3,\tau_4) + \dots\ . \tag{3.9}$$

The function $\mathcal{F}$ contains what are known as ladder diagrams; see Figure 3.4 for a $q = 4$ example. We start with the zero rung diagrams, shown in Figure 3.3, which are just propagators between fermions of different indices:

[4]Where we employ the usual notation $\tau_{12} \equiv \tau_1 - \tau_2$.

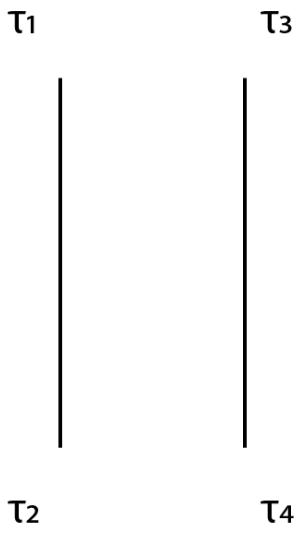

Figure 3.2: The leading piece $G(\tau_{12})G(\tau_{34})$ in the $1/N$ expansion of the four-point function for the SYK model.

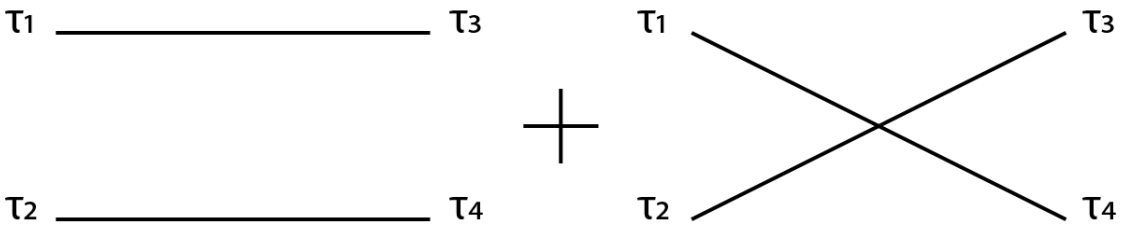

Figure 3.3: The two zero rung base diagrams for the $1/N$ piece of the SYK four-point function. These pieces contribute at order $1/N$ because they mix fermion indices, setting them all equal. Their contribution to the four-point function is $(1/N)\mathcal{F}_0$.

$$\mathcal{F}_0(\tau_1, \tau_2, \tau_3, \tau_4) = -G(\tau_{13})G(\tau_{24}) + G(\tau_{14})G(\tau_{23}) \,, \tag{3.10}$$

where the minus sign comes from anti-commuting the fermions. At first glance, these diagrams would seem to be of order 1 as with the first diagram from above, but there are only N of each of them since propagating from the i fermion to the j fermion can only happen if $i = j$. Thus, only one of the factors of N from the average is canceled.

The next ladder diagram has one rung, building[5] off of the diagram with propagators from τ_1 to τ_3 and τ_2 to τ_4. An example is shown in Figure 3.5. To analyze this diagram, notice that the $q-2$ propagators between the vertices all have completely

[5]Note that the ladder diagrams shown in the figures will all build off of the $\tau_1 \to \tau_3$, $\tau_2 \to \tau_4$ base, but the other base from Equation (3.10) also gives contributing diagrams at $O(1/N)$.

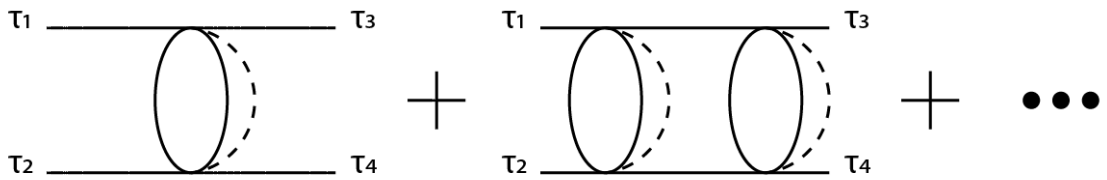

Figure 3.4: Part of the sum of ladder diagrams for the $q = 4$ SYK model. The rest of the sum is given by the same ladder structure built on the second base of Figure 3.3. Each of these diagrams contributes at $O(1/N)$.

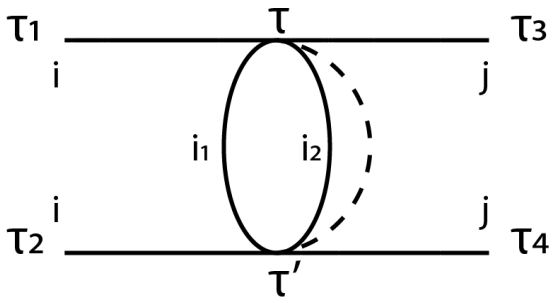

Figure 3.5: A closer look at one of the one rung diagrams for the $q = 4$ SYK model. The fermion index of each propagator is labeled, where the internal indices are summed over and the intermediate times τ and τ' are integrated over.

undetermined fermion indices. Thus, this diagram contributes at order

$$\frac{1}{N^2}\sum_{i_1,\ldots,i_{(q-2)},i,j=1}^{N}\langle j^2_{i_1\ldots i_{(q-2)}ij}\rangle = \frac{1}{N^2}N^q\frac{J^2(q-1)!}{N^{(q-1)}} = \frac{J^2(q-1)!}{N}\,. \tag{3.11}$$

The full contribution from this single-rung ladder diagram is then

$$\mathcal{F}_1^{(1)}(\tau_1,\tau_2,\tau_3,\tau_4) = J^2(q-1)\int d\tau d\tau' \left[G(\tau_1-\tau)G(\tau_2-\tau')G(\tau'-\tau)^{(q-2)}G(\tau-\tau_3)G(\tau'-\tau_4)\right]\,, \tag{3.12}$$

where the contribution from the vertex is as in Equation (3.11), except a $(q-2)!$ symmetry factor from the middle propagators has been divided out. There is another contribution to $\mathcal{F}_1$ which uses the second piece of $\mathcal{F}_0$ as the base on which to add the rung of the ladder, such that

$$\mathcal{F}_1(\tau_1,\tau_2,\tau_3,\tau_4) = \mathcal{F}_1^{(1)}(\tau_1,\tau_2,\tau_3,\tau_4) - \mathcal{F}_1^{(1)}(\tau_1,\tau_2,\tau_4,\tau_3)\,. \tag{3.13}$$

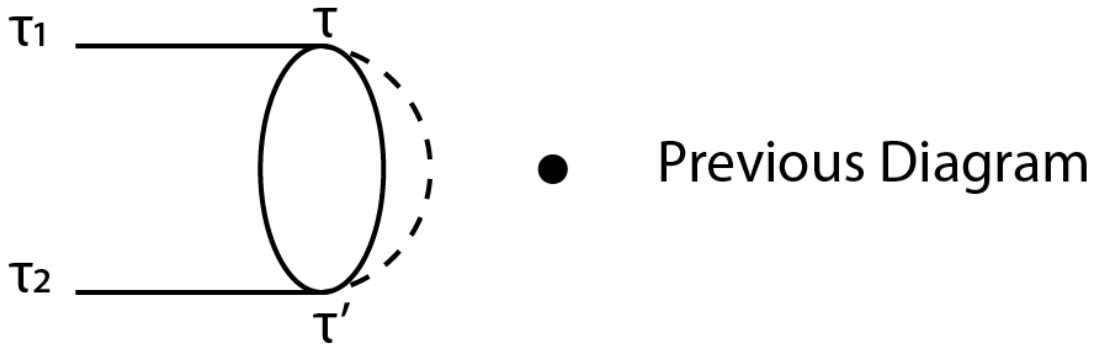

Figure 3.6: A schematic representation of the kernel's action to generate the entire set of ladder diagrams for the SYK model with $q = 4$. The kernel is simply appended to the previous diagram as the new bottom rung.

All of the contributions to the $1/N$ piece are ladder diagrams with different numbers of rungs, so we can write

$$\mathcal{F} = \sum_{n=0}^{\infty} \mathcal{F}_n \ , \tag{3.14}$$

where n denotes the number of rungs. Instead of computing each of these diagrams directly and then summing, we can use the repetitive ladder structure to simplify the calculation. Notice that, to get $\mathcal{F}_{n+1}$, all that must be added to each diagram in $\mathcal{F}_n$ is the bottom rung of a ladder, called the kernel K. This process is pictured in Figure 3.6. The value of K is given by the diagram shown in the figure:

$$K(\tau_1, \tau_2, \tau_3, \tau_4) = -J^2(q-1)G(\tau_{13})G(\tau_{24})G(\tau_{34})^{q-2} \ . \tag{3.15}$$

Then, the next term in the sum $\mathcal{F}_{(n+1)}$ can be constructed from the last by placing the two vertices of the kernel at any value of τ:

$$\mathcal{F}_{(n+1)}(\tau_1, \tau_2, \tau_3, \tau_4) = \int d\tau d\tau' K(\tau_1, \tau_2, \tau, \tau')\mathcal{F}_n(\tau, \tau', \tau_3, \tau_4) \ . \tag{3.16}$$

This equation is of the form of matrix multiplication, so by analogy we can write

$$\mathcal{F} = \sum_n K^n \cdot \mathcal{F}_0 = \frac{1}{1-K} \cdot \mathcal{F}_0 \ , \tag{3.17}$$

where the "$\cdot$" denotes the product of Equation (3.16) and we have summed the geometric series in K. Now, if we could diagonalize K, we could write this equation in terms of its eigenvalues. However, it is not clear that K should be diagonalizable

because it is not symmetric[6]. This can be remedied by conjugating K by powers of the propagator to make a symmetric version,

$$\begin{aligned}\tilde{K} &= |G(\tau_{12})|^{\frac{q-2}{2}} K |G(\tau_{34})|^{\frac{2-q}{2}} \\ &= -J^2(q-1)|G(\tau_{12})|^{\frac{q-2}{2}} G(\tau_{13})G(\tau_{24})|G(\tau_{34})|^{\frac{q-2}{2}} \ ,\end{aligned} \tag{3.18}$$

which shows that K can be diagonalized.

3.1.2 The $1/q$ Expansion

We now begin our study of the $q \to \infty$ limit of the SYK model, following [12] and [13]. We will need to use the Lagrangian for the SYK model, which is

$$L = -\frac{1}{2}\sum_{i=1}^{N} \psi_i \partial_t \psi_i - \sum_{1 \le i_1 < \cdots < i_q \le N} j_{i_1 \ldots i_q} \psi_{i_1} \cdots \psi_{i_q} \ . \tag{3.19}$$

Now, using the replica method, where n copies of the fermions ψ_i are introduced, it was shown in [12] that the action for the (replica) theory is

$$S = -\frac{1}{2}\sum_{a=1}^{n}\sum_{i=1}^{N} \int dt \psi_i^a(t)\partial_t \psi_i^a(t) - \frac{J^2}{2qN^{q-1}} \int dt_1 dt_2 \sum_{a,b=1}^{n} \left(\sum_{i=1}^{N} \psi_i^a(t_i)\psi_i^b(t_2) \right)^q \tag{3.20}$$

We introduce a bi-local collective field

$$\psi^{a,b}(t_1,t_2) = \frac{1}{N}\sum_{i=1}^{N} \psi_i^a(t_1)\psi_i^b(t_2) \equiv \Psi(X,Y) \ , \tag{3.21}$$

where the variables $X = (a, t_1)$ and $Y = (b, t_2)$ are introduced to simplify notation. Switching X and Y gives a minus sign because the ψ are all fermions, so Ψ is anti-symmetric. The replica action above then becomes the effective action

$$S[\Psi] = -\frac{N}{2}\int dX \partial_{t_1} \Psi(X,Y)|_{Y\to X} + \frac{N}{2}\,\mathrm{Tr}[\log(\Psi)] - \frac{NJ^2}{2q}\int dX dY (\Psi(X,Y))^q \ , \tag{3.22}$$

where the integral over X is understood to be an integral over t_1 and a sum over the replicas. The trace-log term comes from changing variables in the measure of the path integral.

[6] Symmetric in the sense of $K(\tau_1,\tau_2,\tau_3,\tau_4)^T = K(\tau_3,\tau_4,\tau_1,\tau_2)$.

To take the $q \to \infty$ limit, we must use the rescaled coupling $\mathcal{J}^2 = \frac{q}{2^{q-1}} J^2$ as defined above, since $\mathcal{J}$ is independent of q. Using this variable, the coefficient of the third term of Equation (3.22) becomes $\frac{2^{q-2}\mathcal{J}^2 N}{q^2}$. We also must redefine our bi-local field to be

$$\Psi(X,Y) = \frac{\text{sgn}(t_{12})}{2}\left[1 + \frac{\Phi(X,Y)}{q}\right] . \tag{3.23}$$

Using the identities

$$\begin{aligned} \frac{\text{sgn}(t_{12})}{2} &= \theta(t_{12}) - \frac{1}{2} , \\ \left(\frac{\text{sgn}(t_{12})}{2}\right)^{-1} &= \partial_{t_1}\delta(t_{12}) , \end{aligned} \tag{3.24}$$

we can rewrite the trace-log term as

$$\begin{aligned} \text{Tr}\log(\Psi) &= \text{Tr}\left[\log\left(\frac{\text{sgn}(t_{12})}{2}\right) + \log\left(1 + \frac{\partial_{t_1}(\text{sgn}(t_{12})\Phi(X,Y))}{2q}\right)\right] \\ &= \text{Tr}\left[\log\left(\frac{\text{sgn}(t_{12})}{2}\right)\right] - \sum_{n=1}^{\infty}\frac{1}{n}\left(\frac{-1}{2q}\right)^n \text{Tr}\left[\partial_{t_1}(\text{sgn}(t_{12})\Phi(X,Y))\right]_*^n , \end{aligned} \tag{3.25}$$

where the power in the last term is to be interpreted as a matrix power, such that $\text{Tr}[f(a,b)]_*^n = \int dadc_1 \ldots dc_{n-1} f(a,c_1)f(c_1,c_2)\cdots f(c_{n-1},a)$. For the interaction term, since we only consider even q, we get

$$(\Psi(X,Y))^q = \frac{1}{2^q}\left[1 + \frac{\Phi(X,Y)}{q}\right]^q , \tag{3.26}$$

but we would like to express this as a power series in $1/q$. Guessing that

$$\left[1 + \frac{\Phi(X,Y)}{q}\right]^q = e^{\Phi(X,Y)}\left[1 + \frac{c_1(X,Y)}{q} + \frac{c_2(X,Y)}{q^2} + O(1/q^3)\right] , \tag{3.27}$$

we can take the log of both sides and keep terms up to $O(1/q^2)$. Doing this yields

$$\begin{aligned} c_1(X,Y) &= -\frac{1}{2}\Phi(X,Y)^2 , \\ c_2(X,Y) &= \frac{1}{3}\Phi(X,Y)^3 + \frac{1}{8}\Phi(X,Y)^4 , \end{aligned} \tag{3.28}$$

such that the collective action is now

$$S[\Phi] = -\frac{N}{2}\sum_{n=2}^{\infty}\frac{1}{n}\left(\frac{-1}{2q}\right)^n \mathrm{Tr}\left[\partial_{t_1}(\mathrm{sgn}(t_{12})\Phi(X,Y))\right]_*^n - \\ -\frac{\mathcal{J}^2 N}{4q^2}\int dXdY e^{\Phi(X,Y)}\left[1+\frac{c_1(X,Y)}{q}+\frac{c_2(X,Y)}{q^2}+O(1/q^3)\right] , \qquad (3.29)$$

where the terms below $O(1/q^2)$ are zero because of the free field equation of motion.

If we restrict ourselves to the $O(1/q^2)$ terms in this action, we get the Liouville action:

$$S_L[\Phi] = -\frac{N}{8q^2}\int dXdY\left[\frac{1}{2}\partial_{t_1}(\mathrm{sgn}(t_{12})\Phi(X,Y))\partial_{t_2}(\mathrm{sgn}(t_{21})\Phi(Y,X)) + 2\mathcal{J}^2 e^{\Phi(X,Y)}\right] . \qquad (3.30)$$

Thus, studying the large q limit of the SYK model is the same as studying the Liouville theory.

3.1.3 The $q \to \infty$ Limit

Equation (3.7) gives a way to analyze the SYK model in the limit of large q. If we consider the infinite temperature limit, the conformal two-point function of Equation (3.6) becomes

$$G_c(\tau) = \frac{b}{|\tau|^{2/q}}\mathrm{sgn}(\tau) . \qquad (3.31)$$

In terms of the variable $\theta = \frac{2\pi\tau}{\beta}$, then, the large q two-point function would simplify to

$$G(\theta) = \frac{\mathrm{sgn}(\theta)}{2} . \qquad (3.32)$$

Since G is the sign function, the part of the four-point function we are considering satisfies the following differential equation:

$$\left[-\frac{\partial_y^2}{4}+v^2\partial_{\tilde{x}}^2-\frac{v^2\tilde{P}^2}{2}\right]\mathcal{F}(x,y,x',y') = \delta(y-y')\delta(x-x')+\delta(y-y'-\pi)\delta(2\pi-x-x') , \qquad (3.33)$$

where $x \equiv \theta_{12}$, $y \equiv \frac{\theta_1+\theta_2}{2}$, $\tilde{P} \equiv \frac{1}{\sin(\tilde{x}/2)}$, $\tilde{x} \equiv vx + (1-v)\pi$, and v is defined implicitly through $\beta\mathcal{J} = \frac{\pi v}{\cos(\pi v/2)}$. These coordinates overcount the physical configurations of states, so to correct for this we only consider the region $x \geq 0$, $x' \geq 0$, and $y \geq y'$.

This equation can be solved by separation of variables: consider first the operator $-\partial_{\tilde{x}}^2 + \tilde{P}^2/2$, with the boundary condition of zero at $x = 0$. In the limit that v goes to one ($\beta\mathcal{J}$ goes to infinity, or strong coupling), a complete set of eigenfunctions for this operator is

$$f_n(\tilde{x}) = \frac{\sin(n\tilde{x})}{\tan(\tilde{x}/2)} - n\cos(n\tilde{x}/2) \ , \tag{3.34}$$

where $n \geq 2$ is an integer. The corresponding eigenvalues are $n^2/4$, as can be easily verified. These functions satisfy the completeness relations

$$\begin{aligned} \sum_{n>2} \frac{f_n(x)f_n(x')}{\pi(n^2-1)} &= \delta(x-x') \ , \\ \sum_{n>2} (-1)^n \frac{f_n(x)f_n(x')}{\pi(n^2-1)} &= \delta(2\pi - x - x') \ . \end{aligned} \tag{3.35}$$

These properties motivate the ansatz

$$\mathcal{F}(x,y,x',y') = \sum_{n>2} H_n(y-y') \frac{f_n(\tilde{x})f_n(\tilde{x}')}{\pi(n^2-1)} \ , \tag{3.36}$$

where the functions H_n are to be determined. The $\tilde{x}$ part of the Equation (3.33) acts on just the unprimed factor of $f_n(\tilde{x})$ to multiply by a factor of $n^2/4$, while the delta functions involving x on the right-hand-side of Equation (3.33) can be rewritten using Equation (3.35)[7]:

$$\delta(y)\delta(x-x') + \delta(y-\pi)\delta(2\pi - x - x') = \sum_{n>2} v[\delta(y) + (-1)^n \delta(y-\pi)] \frac{f_n(\tilde{x})f_n(\tilde{x}')}{\pi(n^2-1)} \ , \tag{3.37}$$

where the factor of v comes from trading x for $\tilde{x}$ and $y' = 0$. Thus, the result of plugging in the ansatz and equating terms at each value of n yields

$$\left[-\frac{\partial_y^2}{4} - \frac{v^2 n^2}{4} \right] H_n(y) = v[\delta(y) + (-1)^n \delta(y-\pi)] \ . \tag{3.38}$$

This differential equation has two source terms, one at $y = 0$ and one at $y = \pi$. Thus, the solution should be a continuous function that has a discontinuous derivative at the source points. Moreover, the function should be 2π-periodic. Because of

[7]Note that this step is necessary because the right-hand-side of Equation (3.33) does not have a factor of $\mathcal{F}$ to equate term-by-term in the sum.

these conditions, we can reinterpret the discontinuity of the derivative $y = 0$ for a discontinuity at $y = 0^+$ and $y = 2\pi^-$. The functions

$$H_n(y) = -\frac{2}{n\sin(n\pi v)}\left(\cos[nv(y-\pi)] + (-1)^n\cos[nv(|y-\pi|-\pi)]\right) , \tag{3.39}$$

satisfy the constraints.

We are only concerned with the strong coupling limit ($v \to 1$). Expanding in powers of $1 - v$, and using the identity $\frac{1}{1-v} \approx \frac{\beta\mathcal{J}}{2} + 1$, we find

$$\begin{aligned} H_n(y) &= \left[\frac{\beta\mathcal{J}}{2} + 1 - \left(y - \frac{\pi}{2}\right)\partial_y\right]\frac{4\cos(ny)}{\pi n^2} + O\left(\frac{1}{\beta\mathcal{J}}\right),\ 0 < y < \pi \\ H_n(y) &= \left[\frac{\beta\mathcal{J}}{2} + 1 - \left(y - \frac{3\pi}{2}\right)\partial_y\right]\frac{4\cos(ny)}{\pi n^2} + O\left(\frac{1}{\beta\mathcal{J}}\right),\ \pi < y < 2\pi , \end{aligned} \tag{3.40}$$

where $O\left(\frac{1}{\beta\mathcal{J}}\right) \sim O(1-v)$. Using $f_n(\tilde{x}) = f_n(x) + (1-v)(\pi - x)f_n'(x) + \ldots$ and plugging into the ansatz, we find the result

$$\begin{aligned} \mathcal{F}(x, y, x', 0) = &\left[\beta\mathcal{J} - 2\left(-1 + \left(y - \frac{\pi}{2}\right)\partial_y + (x-\pi)\partial_x + (x'-\pi)\partial_{x'}\right)\right] \\ &\times \sum_{|n|\geq 2}\frac{e^{-iny}f_n(x)f_n(x')}{\pi^2 n^2(n^2-1)} , \end{aligned} \tag{3.41}$$

for $0 < y < \pi$, where the substitution of $\pi/2 \to 3\pi/2$ in the third term gives the four-point function in the region $\pi < y < 2\pi$.

3.1.4 The Chaos Bound

We would now like to show that the SYK model saturates the chaos bound $\lambda_L \leq \frac{2\pi}{\beta}$ in the limit $v \to 1$ that we took above. One possible route to this property is through analytically continuing the four-point function that was derived above, but we take a slightly different approach here, due to [11] and [14]. First, we define our OTOC to be

$$F(t_1, t_2) = \mathrm{Tr}[y\psi_i(t_1)y\psi_j(0)y\psi_i(t_2)y\psi_j(0)] , \tag{3.42}$$

where $y = \rho(\beta)^{1/4}$ is a quarter of the thermal density matrix contribution, as it was in the chaos bound discussion above. To analyze the four-point function, we must

now consider it on the thermal circle, where the correct propagators to use are the retarded propagators. The kernel is now defined as

$$K_R(t_1, t_2, t_3, t_4) = J^2(q-1)G_R(t_{13})G_R(t_{24})G_{lr}(t_{34})^{q-2} \ , \tag{3.43}$$

where the propagators are

$$\begin{aligned} G_R(t) &= \theta(t) \ , \\ qJ^2 G_{lr}(t)^{q-2} &= \frac{2\pi^2 v^2}{\beta^2 \cosh^2(\frac{\pi v}{\beta} t)} \ , \end{aligned} \tag{3.44}$$

in the large q limit. This four-point function also obeys the generating equation with the kernel, but it can be simplified in this case. When t_1 and t_2 are large, the zero-rung contribution to the propagator is small compared to the other diagrams. Thus, if we consider the sum of the diagrams that contribute to the four-point function, adding a rung to every diagram does not change the sum, since it merely eliminates the contribution from the zero-rung portion. Thus, F is an eigenfunction of the kernel K_R with eigenvalue one:

$$F(t_1, t_2) = \int dt_3 dt_4 K_R(t_1, t_2, t_3, t_4) F(t_3, t_4) \ , \tag{3.45}$$

We now look for solutions of the eigenvalue equation with the form

$$F(t_1, t_2) = e^{\lambda_L (t_1 + t_2)/2} f(t_{12}) \ . \tag{3.46}$$

Since the propagator G_R is just a theta function, if we take the ∂_{t_1} and ∂_{t_2} derivatives on both sides we kill the integrals. We can then rewrite this differential equation in terms of the variable x, defined earlier, as

$$\left[\frac{\lambda_L^2}{4} - \partial_x^2 \right] f(x) = \frac{2\pi^2 v^2}{\beta^2 \cosh^2(\frac{\pi v}{\beta} x)} \ . \tag{3.47}$$

Re-scaling using $\tilde{x} = \frac{\pi v}{\beta} x$ and $\tilde{f}(\tilde{x}) = f(x)$ and re-arranging gives the familiar equation

$$-\left(\frac{\lambda_L \beta}{2\pi v} \right)^2 \tilde{f}(\tilde{x}) = \left[-\partial_{\tilde{x}}^2 - \frac{2}{\cosh^2 \tilde{x}} \right] \tilde{f}(\tilde{x}) \ , \tag{3.48}$$

which is just the Schrödinger equation with a $-\frac{2}{\cosh^2 \tilde{x}}$ potential. This equation is known to only have one bound state, which has energy -1. Thus, it must be the case that

$$\lambda_L = \frac{2\pi}{\beta} v \ , \tag{3.49}$$

so that the SYK model saturates the chaos bound in the $v \to 1$ limit.

3.2 The Spectral Form Factor

The spectral form factor for the SYK model is defined similar to Equation (1.21), except the partition functions are averaged over the disorder[8] [1]:

$$g(\beta, t) \equiv \frac{\langle Z(\beta, t) Z^*(\beta, t) \rangle_J}{\langle Z(\beta) \rangle_J^2} \ , \tag{3.50}$$

where $\langle \cdot \rangle_J$ denotes averaging over the random couplings J. This quantity can be computed numerically by computing each average using many different collections of couplings J. The result is shown in Figure 3.7. The spectral form factor starts to decay, drops to a minimum, then rises back to a plateau. This final rise is called the ramp. As explained in our general discussion of the spectral form factor, the initial decrease and late-time plateau are related to the OTOC and random matrix theory behaviors of the model, respectively. The intermediate-time behavior, including the ramp, are not determined by general considerations, but we will show that they are instead fixed by the quantum chaotic properties of the system.

It would be analytically difficult to calculate the spectral form factor for the SYK model. However, it is a long-standing conjecture that the distribution of eigenvalues of quantum chaotic systems are described by three random matrix models: the Gaussian Unitary Ensemble (GUE), the Gaussian Orthogonal Ensemble (GOE), or the Gaussian Symplectic Ensemble (GSE), depending on the symmetry of the system[9]. It turns out that the GUE reproduces the features of the SYK spectral form factor, as we will now show. Thus, we can study the GUE spectral form factor as a proxy for the SYK model spectral form factor.

3.2.1 The Gaussian Unitary Ensemble

The Gaussian Unitary Ensemble is the set of $N \times N$ Hermitian matrices H, with the probability density

[8] This section follows the discussions in [1] and [2].

[9] Indeed, the first hints of the connection were discovered by Wigner in the 1950s. This relationship has been confirmed in many different examples: see, for example, [15].

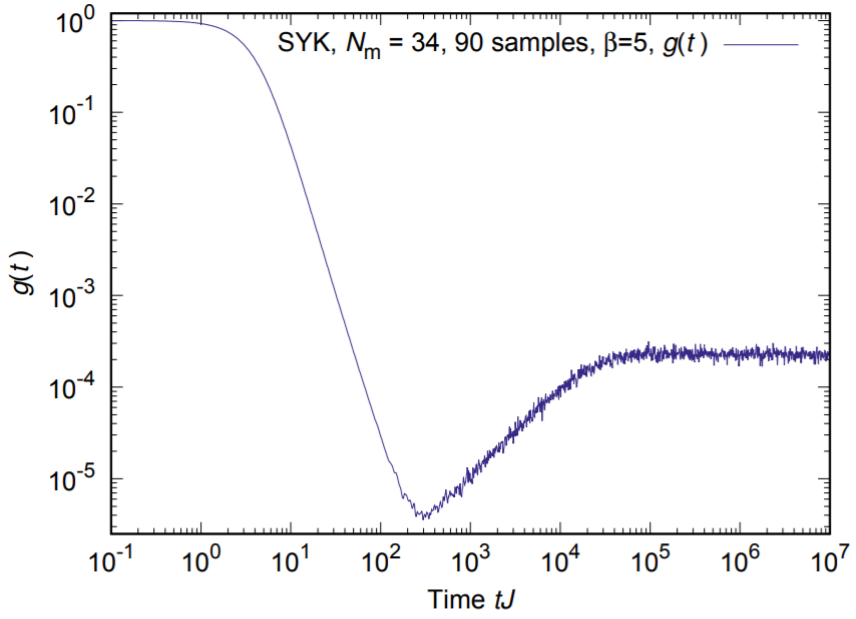

Figure 3.7: A plot of the spectral form factor for the SYK model as numerically calculated in [1]. The interesting intermediate-time behavior of the spectral form factor is due to the SYK model being quantum chaotic.

$$P(H) = \frac{1}{Z} e^{-\frac{N}{2}\operatorname{Tr}(H^2)} , \tag{3.51}$$

where Z is a normalization factor that ensures that this is a probability density. We can compute this Z by integrating $ZP(H)$ over all Hermitian matrices:

$$Z = \int dH e^{-\frac{N}{2}\operatorname{Tr}(H^2)} , \tag{3.52}$$

where the measure is defined as N^2 integrals over real variables:

$$dH = \left(\prod_{i<j}^{N} d(\operatorname{Re} H_{ij}) d(\operatorname{Im} H_{ij}) \right) \left(\prod_{k=1}^{N} dH_{kk} \right) . \tag{3.53}$$

Since the matrix elements of the product are $H^2_{kk} = \sum_j H_{kj} H_{jk} = \sum_j H^*_{jk} H_{jk} = \sum_j (\operatorname{Re} H_{jk})^2 + (\operatorname{Im} H_{jk})^2$, we just have N^2 Gaussian integrals in Equation (3.52), where the off-diagonal integrals have an extra factor of 2 in the exponential compared to the diagonal elements. Thus, $Z = \left(\frac{2\pi}{N}\right)^{N/2} \left(\frac{\pi}{N}\right)^{N(N-1)/2}$, or

$$Z = 2^{N/2} \left(\frac{\pi}{N}\right)^{N^2/2} . \tag{3.54}$$

This analysis additionally reveals that each independent variable in the matrix H is Gaussian distributed with mean zero and standard deviation $1/N$. As in the SYK model, then, we can define a disorder average of the quantity $A(H)$ by

$$\langle A(H)\rangle = \frac{\int dH e^{-\frac{N}{2}\mathrm{Tr}\left(H^2\right)} A(H)}{\int dH e^{-\frac{N}{2}\mathrm{Tr}(H^2)}} \,. \tag{3.55}$$

We use the disorder average to define the spectral form factor as we did for the SYK model (except we omit the normalization factor in the denominator):

$$g(\beta,t) \equiv \langle Z^*(\beta,t)Z(\beta,t)\rangle = \langle \mathrm{Tr}\left[e^{-(\beta+it)H}\right] \mathrm{Tr}\left[e^{-(\beta-it)H}\right]\rangle \,. \tag{3.56}$$

The spectral form factor for the Gaussian Unitary Ensemble can also be calculated numerically. Figure 3.8 shows $g(5,t)$ for $N = 50$, where the matrices H have been normalized in such a way[10] that the eigenvalues lie between -2 and 2 and follow the Wigner semi-circle distribution [1, 2, 16, 17]. To calculate this spectral form factor, 1000 random matrices were diagonalized; the eigenvalues were used to compute the individual spectral form factors, which were then averaged. Figure 3.8 numerically confirms the previously mentioned link between the GUE and SYK spectral form factors.

We now follow [2] in calculating the GUE spectral form factor analytically. Since the measure dH is unchanged under $H \to -H$, if $\beta \to -\beta$, the extra signs introduced from this change can always be removed by flipping H. Thus, $g(\beta,t) = g(-\beta,t)$ is an even function in β. Additionally, g was defined to be an even function in t, so without loss of generality we can restrict to the region $\beta \geq 0$, $t \geq 0$. As previously mentioned, the distribution of eigenvalues $\rho(\mu)$ of the Hermitian matrices of the GUE model will be normalized to lie between -2 and 2, such that they follow the Wigner semi-circle distribution

$$\rho(\mu) = \frac{1}{2\pi}\sqrt{4-\mu^2} \,. \tag{3.57}$$

The trick to analytically computing the spectral form factor is noticing that the defining integral equation for $g(\beta,t)$ is mathematically equivalent to that of the correlator of 1/2 Bogomol'nyi-Prasad-Sommerfeld (BPS) Wilson loops[11] in four dimensional $\mathcal{N} = 4$ supersymmetric Yang-Mills (SYM) theory. We can simply port this known result from [18] after changing variables. The first change we make is

[10] For $N = 50$, this normalization factor can be numerically determined to be $H \to H/500$. See the Code Appendix for details on the specific calculation of the spectral form factor shown here.

[11] The correlator for 1/2 BPS Wilson loops is also defined using an average over the GUE random matrices; see Equation (3.61)

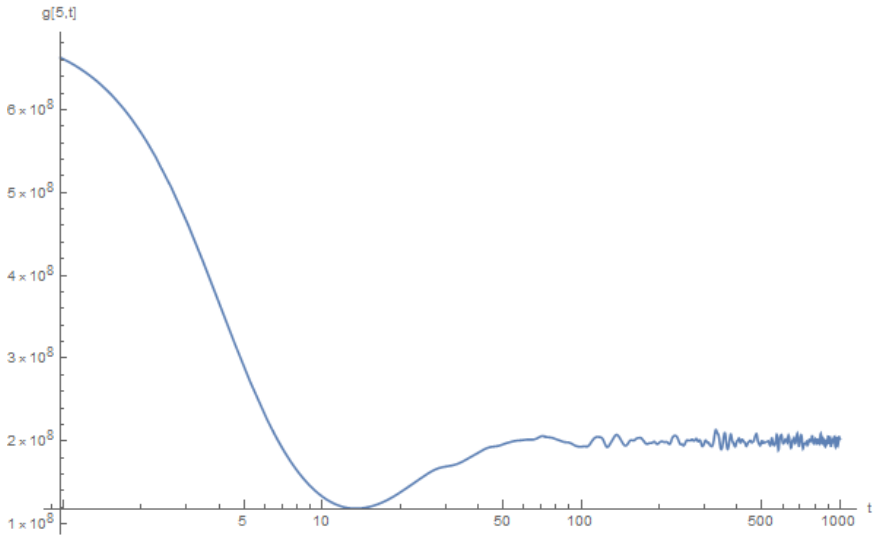

Figure 3.8: A plot of the spectral form factor for the Gaussian Unitary Ensemble for $N = 50$ and $\beta = 5$ using 1000 randomly generated matrices. The plateau of this spectral form factor is again slightly fuzzy because of the noise inherent in averaging over the random matrix ensemble. References [1] and [2] give additional plots of the GUE spectral form factor for different parameter values.

$$H \equiv \sqrt{\frac{2}{N}} M \,, \tag{3.58}$$

where the constant factor relating the measures dM and dH cancel because of the division in Equation (3.55). Additionally, this simplifies the probability density weight factor (by design):

$$e^{-\frac{N}{2}\,\mathrm{Tr}\left(H^2\right)} = e^{-\,\mathrm{Tr}\left(M^2\right)} \,. \tag{3.59}$$

To rewrite the definition of the GUE spectral form factor in terms of this M, we just include the appropriate constants in the exponential

$$g(\beta, t) = \left\langle \mathrm{Tr}\left[e^{-\frac{(\beta+it)\sqrt{2}}{\sqrt{N}}M}\right] \mathrm{Tr}\left[e^{-\frac{(\beta-it)\sqrt{2}}{\sqrt{N}}M}\right] \right\rangle \,. \tag{3.60}$$

The expression for the correlator of 1/2 BPS Wilson loops is

$$\left\langle \prod_i e^{k_i \sqrt{\frac{\lambda}{4N}}\sqrt{2}M} \right\rangle \,, \tag{3.61}$$

where the k_i are the winding numbers. For our purposes, $i = 1, 2$, and $k_1\sqrt{\lambda} \equiv -2(\beta + it)$, $k_2\sqrt{\lambda} \equiv -2(\beta - it)$. To write down this correlator, we will use the symmetric matrix $A(z)$, defined by

$$A(z)_{i,j} = \sqrt{\frac{i!}{j!}} e^{z^2/2} z^{j-i} L_i^{j-i}(-z^2) \ , \tag{3.62}$$

where i and j range from 0 to $N-1$ and L_i^{j-1} is the associated Laguerre polynomial. The first correlator we are interested in is the one-point function[12]:

$$\left\langle \mathrm{Tr}\left(e^{z\sqrt{2}M}\right)\right\rangle = \mathrm{Tr}(A(z)) = e^{\frac{z^2}{2}} L_{N-1}^1(-z^2) \ . \tag{3.63}$$

The one-point function is used in the definition of the disconnected part of the spectral form factor g_d, defined as

$$g_d(\beta,t) \equiv \langle Z(\beta,t)\rangle\langle Z^*(\beta,t)\rangle = \left\langle \mathrm{Tr}\left[e^{-\frac{(\beta+it)\sqrt{2}}{\sqrt{N}}M}\right]\right\rangle \left\langle \mathrm{Tr}\left[e^{-\frac{(\beta-it)\sqrt{2}}{\sqrt{N}}M}\right]\right\rangle \tag{3.64}$$

Making the identifications $z = -\frac{\beta+it}{\sqrt{N}}$ and $\bar{z} = -\frac{\beta-it}{\sqrt{N}}$, we can use the BPS result from Equation (3.63) to write

$$g_d(\beta,t) = e^{\frac{(z^2+\bar{z}^2)}{2}} L_{N-1}^1(-z^2) L_{N-1}^1(-\bar{z}^2) \ . \tag{3.65}$$

The exact[13] disconnected part of the GUE spectral form factor that we considered before is plotted in Figure 3.9. The disconnected part, then, is responsible for the early-time behavior of the spectral form factor and is negligible at late times.

To study the late-time behavior of the spectral form factor, then, we need to study the part of the spectral form factor that is not g_d. This part is the connected part, defined as

$$g_c(\beta,t) = g(\beta,t) - g_d(\beta,t) \ . \tag{3.66}$$

In the BPS analysis of [18], the connected part of the 1/2 Wilson loop BPS correlator, and by analogy g_c, is shown to be

$$g_c(\beta,t) = \mathrm{Tr}[A(z+\bar{z}) - A(z)A(\bar{z})] \ . \tag{3.67}$$

Consider $\mathrm{Tr}[A(z+\bar{z})] = \mathrm{Tr}\left[A(-\frac{2\beta}{\sqrt{N}})\right]$. This portion is independent of time, so it must set the value of the plateau for the spectral form factor:

[12]Which can be calculated by noticing that the matrix elements of A can be written in terms of the raising and lowering operators of the harmonic oscillator, as in Appendix A of [2].

[13]We stress that Figure 3.9 is not numerically calculated, but is the plot of Equation (3.65) for the parameter values considered above.

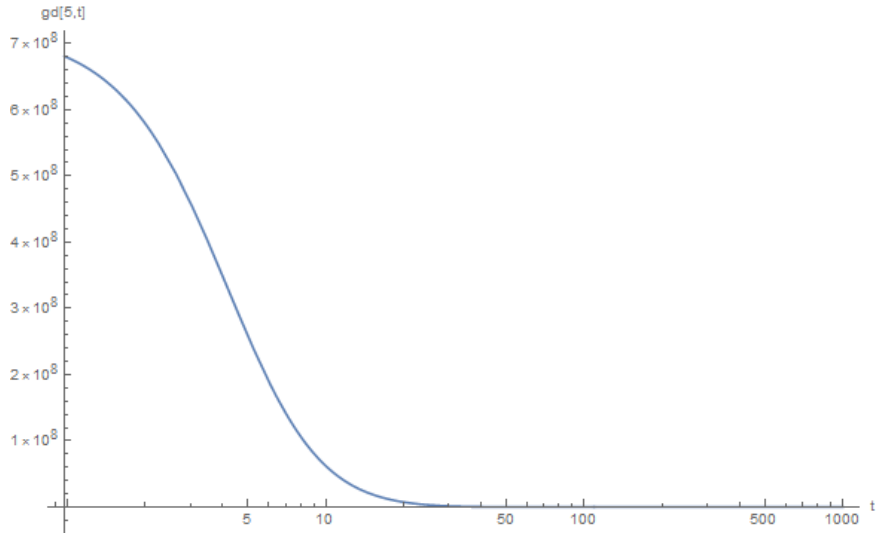

Figure 3.9: A plot of the exact disconnected part of the spectral form factor for the Gaussian Unitary Ensemble for $N = 50$ and $\beta = 5$. It is clear that the disconnected part is responsible for the behavior of the spectral form factor at early times only.

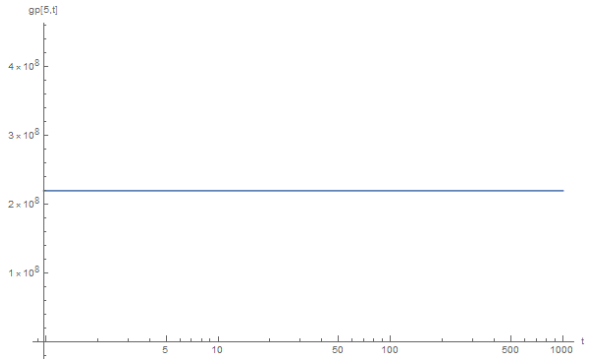

Figure 3.10: A plot of the exact plateau part of the connected piece of the spectral form factor for the Gaussian Unitary Ensemble for $N = 50$ and $\beta = 5$.

$$g_p(\beta, t) = \mathrm{Tr}\left[A\left(-\frac{2\beta}{\sqrt{N}}\right)\right] = e^{\frac{2\beta^2}{N}} L^1_{N-1}\left(-\frac{4\beta^2}{N}\right) . \tag{3.68}$$

The constant plateau function is plotted for $\beta = 5$ and $N = 50$ in Figure 3.10.

We can manually construct the matrix $A(z)$ and plot the entire connected piece of the spectral form factor for the case $\beta = 5$ and $N = 50$: the result of this procedure is shown[14] in Figure 3.11. The shape is as expected, and it implies that $g_r(\beta, t) \equiv -\mathrm{Tr}[A(z)A(\bar{z})]$ is negative and describes the ramp of the spectral form

[14]We now use MATLAB for calculations and plotting because of a numerical difficulty in the Mathematica implementation where the spectral form factor wildly oscillated starting at $t = 30$. Because a number of consistency checks were satisfied in the region away from $t = 30$, we suspect numerical precision was being lost near $t = 30$ for an unknown reason.

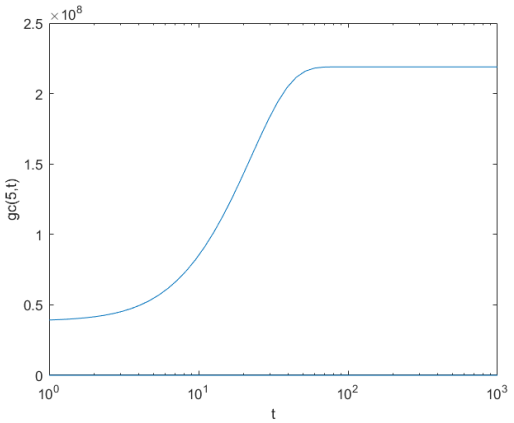

Figure 3.11: A plot of the exact connected piece of the spectral form factor for the Gaussian Unitary Ensemble for $N = 50$ and $\beta = 5$.

factor. Figure 3.12 puts all of these results together and shows the exact spectral form factor for $\beta = 5$ and $N = 50$.

3.2.2 Slope of the Ramp

We will now briefly describe the result of the calculation of the slope of $g_r(\beta, t)$ as carried out in [2] because of its connection to random matrix theory. First, since g_p, the plateau piece, is a constant, it is independent of time. Thus, since $g_c(\beta, t) = g_p(\beta, t) + g_r(\beta, t)$,

$$\frac{\partial g_r}{\partial t} = \frac{\partial g_c}{\partial t} \ . \tag{3.69}$$

From the same general considerations that lead to Equation (3.67), the time derivative of g_c can be calculated to be

$$\frac{\partial g_c}{\partial t}(\beta, t) = \frac{N}{\beta} e^{\frac{(z^2+\bar{z}^2)}{2}} \operatorname{Im}[L_N(-z^2)L_{N-1}(-\bar{z}^2)] \ , \tag{3.70}$$

where L_α is the Laguerre polynomial. The function $s(\beta, t)$, defined using the time derivative of g_c as

$$s(\beta, t) \equiv \frac{1}{4\beta} \operatorname{arcsinh}\left(2\pi\beta \frac{\partial g_c}{\partial t}(\beta, t)\right) \ , \tag{3.71}$$

can be shown to obey the semi-circle law:

$$s(\beta, t)^2 + \tau^2 = 1 \ , \tag{3.72}$$

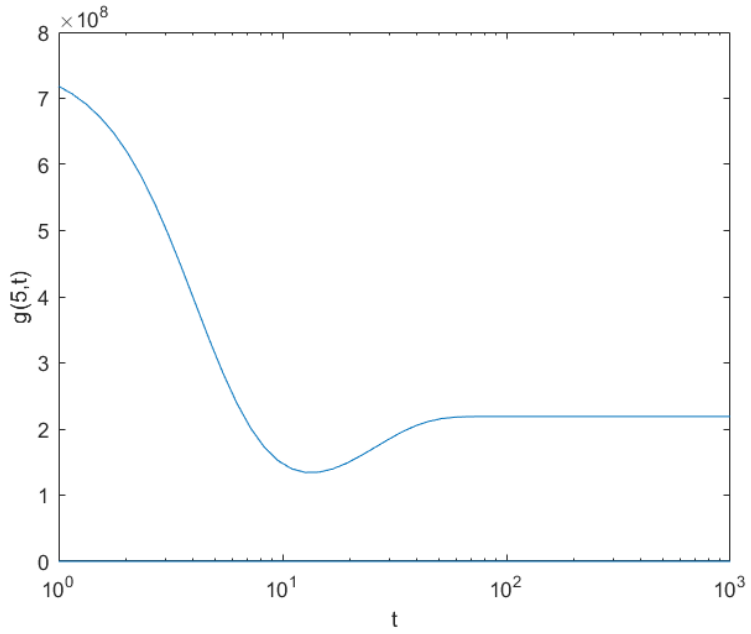

Figure 3.12: A plot of the exact spectral form factor for the Gaussian Unitary Ensemble for $N = 50$ and $\beta = 5$. Compare with the numerically (Monte Carlo) calculated spectral form factor from Figure 3.8.

where $\tau = \frac{t}{2N}$. The significance of this finding is that it confirms that the middle-time behavior of the GUE spectral form factor (the ramp) is controlled by the random matrix theory prediction for the eigenvalue spectrum of the model.

Chapter 4

Conclusions

In this thesis, we have explored the concept of quantum chaos and some of the systems that exhibit it. The tools we used in our study came from two places: the OTOC was motivated directly from the Poisson bracket argument that showed how quantum chaotic systems would be expected to behave, while the spectral form factor was motivated indirectly as a tool to study the discrete spectra of quantum chaotic systems and compare them to random matrix theory ensembles[1]. We applied these concepts first to familiar quantum mechanical systems to test their behavior. There is still much to be explored in the simple quantum mechanical setting, particularly for systems with continuous spectra[2] General results relating classical and quantum chaos seem to be lacking.

The SYK model has attracted much attention over the past few years as an example of a tractable holographic system. Many extensions of the SYK model have been developed, and much effort has been spent trying to understand the various properties of the SYK model [20, 21]. As these motivations suggest, the ultimate hope for quantum chaos is that it will help in understanding quantum gravity, as any theory of quantum gravity describing many-body interactions would be expected to be chaotic. The SYK model itself is related to Jackiw-Teitelboim (JT) gravity, and recent papers have found a connection between non-perturbative JT gravity and matrix integrals [22, 23]. As it stands, studies of quantum chaotic systems are poised to give the best near-term results in quantum gravity, with other surprises and new physics possible along the way.

[1] Spectral form factors were also motivated by the discrete spectrum of black hole microstates.
[2] For an example of a system that could be studied, see [19].

Appendix A

The Schwarz-Pick Theorem

Let D be the open unit disk in the complex plane. The Schwarz-Pick theorem states that, if $f : D \to D$ is holomorphic, then $\forall z_1, z_2 \in D$,

$$\left| \frac{f(z_1) - f(z_2)}{1 - (f(z_1))^* f(z_2)} \right| \leq \left| \frac{z_1 - z_2}{1 - (z_1)^* z_2} \right| . \tag{A.1}$$

Taking the limit as $z_1 \to z_2$, squaring, and multiplying by four gives the preservation or decreasing of distances in the hyperbolic metric, justifying Equation (1.13). To prove the theorem, we first need to prove the Schwarz Lemma: let $g : D \to \mathbb{C}$ be a holomorphic function with $g(0) = 0$ and $\forall z \in D : |g(z)| \leq 1$. Then, $\forall z \in D : |g(z)| \leq |z|$ and $|g'(0)| \leq 1$. Additionally, if $|g(z)| = |z|$ for some $z \neq 0$ in D, or if $|g'(0)| = 1$, then $g(z) \propto z$.

Proving the Schwarz Lemma is an application of the maximum principle for holomorphic functions[1]. Consider the function

$$h(z) = \begin{cases} \frac{g(z)}{z} & z \neq 0 , \\ g'(0) & z = 0 , \end{cases} \tag{A.2}$$

which is holomorphic on the D. It is clearly continuous at zero, since $\lim_{z\to 0} h(z)$, just gives the definition of the complex derivative of g at $z = 0$. It is also clearly differentiable when $z \neq 0$. The only potential problem could be the derivative at $z = 0$, but this is just equal to $g''(0)$, since $h'(0) = \lim_{z\to 0}(g(z)/z^2) - (g'(0)/z)$, and the first term can be approximated by $g'(z)/z$ near $z = 0$. The existence of this derivative ensures that h is holomorphic on D. Now, for any closed disk of radius $r < 1$ centered at zero, for any z in this disk, the maximum principle for h implies that there exists z_0 with $|z_0| = r$ such that

[1]The maximum principle states that holomorphic functions attain their maximum modulus on the boundary of their domain of definition. This follows directly from the maximum principle for harmonic functions.

$$|h(z)| \leq |h(z_0)| \leq \frac{1}{r} \, , \tag{A.3}$$

where the last inequality follows from the bound on $|g|$. Taking the limit as $r \to 1$ gives the Schwarz lemma.

We now use the Schwarz lemma to prove the Schwarz-Pick theorem. Consider, for a fixed $z_0 \in D$, the Möbius transformation

$$M(z) = \frac{z_0 - z}{z_0^* z - 1} \, . \tag{A.4}$$

If $z = e^{i\theta}$, then

$$|M(e^{i\theta})|^2 = \frac{z_0 - z}{z_0^* z - 1} \frac{z_0^* - z^*}{z_0 z^* - 1} = 1 \, , \tag{A.5}$$

since $|z|^2 = 1$. So M maps the unit circle to itself, and thus maps the disk to the disk. Define another Möbius transformation by

$$\phi(z) = \frac{f(z_0) - z}{1 - (f(z_0))^* z} \, . \tag{A.6}$$

Since Möbius transformations are invertible and $M(z_0) = 0$ and $\phi(f(z_0)) = 0$, we can form the composition $\phi(f(M^{-1}(z)))$, which maps zero to zero and maps the unit disk to the unit disk, since ϕ also maps the unit disk to the unit disk (it is of the same form as M, since $|f(z_0)| \leq 1$). Thus, the Schwarz lemma applies to the composition, so if $z = M(z_1)$, then

$$|\phi(f(M^{-1}(z)))| = \left| \frac{f(z_0) - f(z_1)}{1 - (f(z_0))^* f(z_1)} \right| \leq \left| \frac{z_0 - z_1}{1 - z_0^* z_1} \right| \, , \tag{A.7}$$

exactly what we wanted to prove.

Appendix B

Code Appendix

For the benefit of the reader trying to reproduce the results above, we have included here all code used to make the plots in this paper, with a few comments[1]. The languages used were Mathematica and Matlab. The Matlab code will be denoted as such, while all other code is Mathematica. Code will be listed in gray boxes, where line breaks due to line overflow will be denoted by a return arrow.

B.1 Figure 1.1, the Harmonic Oscillator Spectral Form Factor

```
Clear["Global`*"]
beta = 5;
LogLinearPlot[(1 + Exp[-2*beta] - 2*Exp[-beta])/(1 + Exp[-2*beta] - 2*Exp[-beta]*Cos[t]), t, 0, 100,
  ↪ AxesLabel -> "t", "g[5,t]"]
```

B.2 Figure 1.2, an Example of a Continuous Spectrum Hamiltonian's Spectral Form Factor

```
Clear["Global`*"]
beta = 5;
LogLinearPlot[beta^2/(beta^2 + t^2), t, 0, 100,AxesLabel -> "t", "g[5,t]"]
```

[1]Why not a Github repository? While that may seem to be a simpler solution, I worry that it may not be a long-term one. Moreover, I feel the code should be more easily accessible from the paper than a link to a Github repository would be. Finally, I feel the code should be viewed as part of the submission of this thesis and not as an adjacent product.

B.3 Figure 2.1, the Microcanonical OTOC c_1 for the Particle in a Box Hamiltonian

```
Clear["Global`*"];
(* Start with known solution to infinite square well *)
m := 1;
L := 1;
xc := 1/2;
Energy[n_, L_] := n^2 * Pi^2/(2*L);
Psi[n_, L_, x_, xc_] := Sqrt[2/L]*Sin[n*Pi*(x - xc + L/2)/L];
Plot[Psi[1, L, x, xc], x, 0, 1]
Integrate[Abs[Psi[1, L, x, xc]]^2, x, 0, 1]
(* Now calculate xnm *)
opx[n_, m_] := Integrate[Psi[n, L, x, xc]*x*Psi[m, L, x, xc], x, 0, 1];
Simplify[Simplify[opx[k, t], Element[k, Integers]], Element[t, Integers]]
Simplify[Simplify[opx[k, k], Element[k, Integers]]]
Nmax := 50;
Nopx[n_, m_] := Integrate[N[Psi[n, L, x, xc]*x*Psi[m, L, x, xc]], x, 0, 1];
matx = Table[N[Nopx[n, m]], n, 1, Nmax, m, 1, Nmax];
dE[k_, m_] := N[Energy[k, L] - Energy[m, L]];
bmat[n_, m_, t_, Nmax_] := Sum[matx[[n, k]]*matx[[k, m]]*(dE[k, m]*N[Exp[I*dE[n, k]*t]] - dE[n,
  ↪ k]*N[Exp[I*dE[k, m]*t]]), k, 1, Nmax];
Plot[Abs[bmat[1, 1, t, Nmax]], t, 0, 1]
matb := Table[bmat[n, m, t, Nmax], n, 1, Nmax, m, 1, Nmax];
cn[n_, time_] := matb[[n, All]].matb[[All, n]] /. t -> time;
ListPlot[Table[time/100, Chop[cn[1, time/100]], time, 0, 100]]
```

This particular implementation is quite slow[2], and could possibly be improved by not using so many function calls.

[2]This is the reason we chose to ListPlot the result instead of Plot.

B.4 Figure 3.8, the Numerically-Calculated GUE Spectral Form Factor

```
Clear["Global`*"]
nsamples = 1500;
g = 0;
n = 50;
beta = 5;
For[k = 0, k < nsamples + 1, k++,
  data = RandomVariate[NormalDistribution[0, n], n^2];
  H := Table[
    If[i == j,
     If[i == 1, data[[1]],
      data[[Sum[2*n - (2*(k) - 1), k, 1, i - 1] + 1]]],
     If[j > i,
      data[[Sum[2*n - (2*(k) - 1), k, 1, i - 1] + 2 +
         2*Abs[j - i - 1]]] +
       I*data[[Sum[2*n - (2*(k) - 1), k, 1, i - 1] + 3 +
          2*Abs[j - i - 1]]],
      data[[Sum[2*n - (2*(k) - 1), k, 1, j - 1] + 2 +
         2*Abs[i - j - 1]]] -
       I*data[[Sum[2*n - (2*(k) - 1), k, 1, j - 1] + 3 +
          2*Abs[i - j - 1]]]]], i, 1, n, j, 1, n];
  evalH = Eigenvalues[H/500];
  g = g + Total[Exp[-(beta + I t)*evalH]] Total[
      Exp[-(beta - I t)*evalH]];];
g = g/nsamples;
Plot[Abs[g], t, 0, 100]
LogLinearPlot[Abs[g], t, 0, 1000, AxesLabel -> "t", "g[5,t]"]
```

B.5 Figures 3.9 and 3.10, the Disconnected and Plateau Pieces of the GUE Spectral Form Factor

```
beta = 5;
LogLinearPlot[
 Exp[(beta^2 - t^2  )/n] LaguerreL[n - 1,
   1, -(beta + I t)^2/n] LaguerreL[n - 1, 1, -(beta - I t)^2/n], t,
           0, 1000, AxesLabel -> "t", "gd[5,t]", Mesh -> All,
 PlotPoints -> 500]
 LogLinearPlot[
 Exp[2 beta^2 /n] LaguerreL[n - 1, 1, -4 beta^2/n], t, 0, 1000,
 AxesLabel -> "t", "gp[5,t]"]
```

B.6 Figures 3.11 and 3.12, the Connected Piece of the GUE Spectral Form Factor and the Exact GUE Spectral Form Factor

```
t = logspace(0,3,50);
n = 50;
beta = 5;
z = -(beta + 1i*t)/sqrt(n);
zbar = -(beta - 1i*t)/sqrt(n);
Az = zeros(n,n,length(t));
Azbar = zeros(n,n,length(t));
Azpluszbar = zeros(n,n,length(t));
for k = 0:n-1
    for p = 0:n-1
        Az(k+1,p+1,:) =
          ↪ sqrt(factorial(k)/factorial(p))*exp(z.^2/2).*z.^(p-k).*laguerreL(k,p-k,-z.^2);
        Azbar(k+1,p+1,:) = sqrt(factorial(k)/factorial(p))*exp(zbar.^2/2).*zbar.^(p-k).*⌋
          ↪ laguerreL(k,p-k,-zbar.^2);
        Azpluszbar(k+1,p+1,:) = sqrt(factorial(k)/factorial(p))*exp((z+zbar).^2/2).*⌋
          ↪ (z+zbar).^(p-k).*laguerreL(k,p-k,-(z+zbar).^2);
    end
end

gd = zeros(length(t));
for time = 1:length(t)
    gd(time) = trace(Az(:,:,time))*trace(Azbar(:,:,time));
end
figure(1)
semilogx(t,gd);
xlabel('t')
ylabel('gd(5,t)')

gc = zeros(length(t));
for time = 1:length(t);
    gc(time) = trace(Azpluszbar(:,:,time)) - trace(Az(:,:,time)*Azbar(:,:,time));
end
figure(2)
semilogx(t,gc);
xlabel('t')
ylabel('gc(5,t)')

gr = zeros(length(t));
for time = 1:length(t);
    gr(time) = -1*trace(Az(:,:,time)*Azbar(:,:,time));
end
figure(3)
semilogx(t,gr);
xlabel('t')
ylabel('gr(5,t)')

g = gd+gc;
figure(4)
semilogx(t,g);
xlabel('t')
ylabel('g(5,t)')
```

These figures were created with Matlab.

References

[1] J. S. Cotler, G. Gur-Ari, M. Hanada, J. Polchinski, P. Saad, S. H. Shenker, D. Stanford, A. Streicher, and M. Tezuka, "Black holes and random matrices," *Journal of High Energy Physics*, vol. 2017, p. 118, May 2017.

[2] K. Okuyama, "Spectral form factor and semi-circle law in the time direction," *Journal of High Energy Physics*, vol. 2019, p. 161, Feb 2019.

[3] P. Dirac, *The Priciples of Quantum Mechanics*. Oxford, UK: Oxford University Press, 4 ed., 2004.

[4] A. I. Larkin and Y. N. Ovchinnikov, "Quasiclassical Method in the Theory of Superconductivity," *Soviet Journal of Experimental and Theoretical Physics*, vol. 28, p. 1200, June 1969.

[5] B. Michel, J. Polchinski, V. Rosenhaus, and S. J. Suh, "Four-point function in the IOP matrix model," *Journal of High Energy Physics*, vol. 2016, p. 48, May 2016.

[6] J. Maldacena, S. H. Shenker, and D. Stanford, "A bound on chaos," *Journal of High Energy Physics*, vol. 2016, p. 106, Aug 2016.

[7] S. H. Shenker and D. Stanford, "Black holes and the butterfly effect," *Journal of High Energy Physics*, vol. 2014, p. 67, Mar 2014.

[8] B. Bertini, P. Kos, and T. Prosen, "Exact Spectral Form Factor in a Minimal Model of Many-Body Quantum Chaos," *Phys. Rev. Let.*, vol. 121, p. 264101, Dec 2018.

[9] K. Hashimoto, K. Murata, and R. Yoshii, "Out-of-time-order correlators in quantum mechanics," *Journal of High Energy Physics*, vol. 2017, p. 138, Oct. 2017.

[10] J.-G. Hartmann, J. Murugan, and J. P. Shock, "Chaos and scrambling in quantum small worlds," *arXiv preprint arXiv:1901.04561*, 2019.

[11] J. Maldacena and D. Stanford, "Remarks on the sachdev-ye-kitaev model," *Phys. Rev. D*, vol. 94, p. 106002, Nov 2016.

[12] A. Jevicki, K. Suzuki, and J. Yoon, "Bi-local holography in the SYK model," *Journal of High Energy Physics*, vol. 2016, p. 7, Jul 2016.

[13] K. Suzuki, "1/q Expansion of the SYK Model," Sept 2017.

[14] A. Kitaev, "Hidden correlations in the hawking radiation and thermal noise." http://online.kitp.ucsb.edu/online/joint98/kitaev/.

[15] H. Gharibyan, M. Hanada, S. H. Shenker, and M. Tezuka, "Onset of Random Matrix Behavior in Scrambling Systems," *JHEP*, vol. 07, p. 124, 2018. [Erratum: JHEP02,197(2019)].

[16] E. P. Wigner, "Characteristic vectors of bordered matrices with infinite dimensions," *Ann. of Math*, vol. 62, no. 3, pp. 548–564, 1955.

[17] E. P. Wigner, "On the distribution of the roots of certain symmetric matrices," *Ann. Math*, vol. 67, no. 2, pp. 325–327, 1958.

[18] K. Okuyama, "Connected correlator of 1/2 BPS Wilson loops in N=4 SYM," *Journal of High Energy Physics*, vol. 2018, p. 37, Oct 2018.

[19] T. Morita, "Semi-classical bound on Lyapunov exponent and acoustic Hawking radiation in c=1 matrix model," *arXiv e-prints*, p. arXiv:1801.00967, Jan 2018.

[20] J. Murugan, D. Stanford, and E. Witten, "More on supersymmetric and 2d analogs of the SYK model," *Journal of High Energy Physics*, vol. 2017, p. 146, Aug 2017.

[21] P. Saad, S. H. Shenker, and D. Stanford, "A semiclassical ramp in SYK and in gravity," *arXiv e-prints*, p. arXiv:1806.06840, Jun 2018.

[22] P. Saad, S. H. Shenker, and D. Stanford, "JT gravity as a matrix integral," *arXiv e-prints*, p. arXiv:1903.11115, Mar 2019.

[23] J. Maldacena, G. J. Turiaci, and Z. Yang, "Two dimensional Nearly de Sitter gravity," *arXiv e-prints*, p. arXiv:1904.01911, Apr 2019.